IEEE Access
Multidisciplinary | Rapid Review | Open Access Journal

Received September 28, 2017, accepted October 18, 2017, date of publication October 31, 2017, date of current version November 28, 2017.

Digital Object Identifier 10.1109/ACCESS.2017.2768401

Generalized Frequency Division Multiplexing With Flexible Index Modulation

ERSİN ÖZTÜRK[1,2], ERTUGRUL BASAR[1], (Senior Member, IEEE), AND HAKAN ALİ ÇIRPAN[1], (Member, IEEE)

[1]Faculty of Electrical and Electronics Engineering, Istanbul Technical University, 34469 Istanbul, Turkey
[2]Netas Telecommunication, Department of Research and Development, 34912 Istanbul, Turkey

Corresponding author: Ersin Öztürk (ersinozturk@itu.edu.tr)

This work was partially supported by Netas Telecommunication.

ABSTRACT After the vision and the overall objectives of future wireless networks for 2020 and beyond have been defined, standardization activities for fifth generation (5G) wireless networks have been started. Although it is expected that 5G new radio (NR) will be based on cyclicly prefixed orthogonal frequency division multiplexing (CP-OFDM)-based waveforms along with multiple waveform numerologies, the sufficiency of CP-OFDM-based NR is quite disputable due to the continuing massive growth trend in number of wireless devices and applications. Therefore, studies on novel radio access technologies (RATs) including advanced waveforms and more flexible radio accessing schemes must continue for future wireless networks. Generalized frequency division multiplexing (GFDM) is one of the prominent non-CP-OFDM-based waveforms. It has recently attracted significant attention in research because of its beneficial properties to fulfill the requirements of future wireless networks. Multiple-input multiple-output (MIMO)-friendliness is a key ability for a physical layer scheme to satisfactorily match the foreseen requirements of future wireless networks. On the other hand, the index modulation (IM) concept, which relies on conveying additional information bits through indices of certain transmit entities, is an emerging technique to provide better spectral and energy efficiency. In this paper, considering the advantages of non-CP-OFDM-based waveforms and the IM concept, we present a framework, which integrates GFDM with space and frequency IM schemes to provide flexible and advanced novel RATs for future wireless networks. Several MIMO-GFDM schemes are provided through the proposed framework and their bit error ratio performances, computational complexities, and spectral efficiencies are analyzed. Based on the obtained results, a guideline for selecting the proper MIMO-GFDM scheme considering target performance criterion is given. It has been demonstrated that the proposed framework has a strong potential to engineer the space-frequency structure according to channel conditions and use cases, and it provides a great flexibility that can be easily tuned to address the required performance criterion.

INDEX TERMS 5G wireless networks, GFDM, index modulation, MIMO systems, multicarrier modulation, physical layer design, quadrature spatial modulation, spatial modulation.

I. INTRODUCTION

Wireless communications has become an essential tool for our life. Starting from the first generation wireless networks (1G), there has been an exponential growth in number of users and their applications. Owing to a broad range of applications spanning from wireless regional area networks to machine type communications, future wireless networks have challenging objectives such as very high spectral and energy efficiency, very low latency and very high data rate, which require more effective physical layer (PHY) solutions [1]. In this context, the vision and overall objectives of future wireless networks for 2020 and beyond have been defined by the International Telecommunication Union [2] and standardization activities for fifth generation (5G) wireless networks have been started through discussions about scenarios and requirements by Third Generation Partnership Project (3GPP) [3].

Orthogonal frequency division multiplexing (OFDM) is the core of the physical layer of fourth generation (4G) wireless networks and fulfills the requirements and challenges of 4G scenarios. Despite of its proven advantages, OFDM has some shortcomings that make it difficult to address the scenarios foreseen for future 5G wireless networks. In OFDM, every symbol requires a cyclic prefix (CP), which

depends on the tap length of the channel. The insertion of CP reduces the spectral efficiency and prevents obtaining a low latency by shortening the symbols. Furthermore, OFDM is very sensitive to time and frequency synchronization errors and has high out-of-band (OOB) emission due to rectangular pulse shaping. Thus, OFDM can fulfill the requirements of 5G wireless networks in a limited way.

In recent years, several waveform proposals have been presented to overcome the above limitations of OFDM. These proposals can be categorized into two main classes: cyclicly-prefixed OFDM (CP-OFDM)-based and non-CP-OFDM-based. The proposals in the first class, such as filtered OFDM (f-OFDM) [4], [5] and windowed OFDM (W-OFDM) [6], are the attempts to resolve the aforementioned problems by keeping the orthogonality. The proposals in the second class initially dismiss orthogonality to obtain better temporal and spectral characteristics, thus, causes a major paradigm shift in the context of waveform design, which may yield some backward compatibility issues.

Generalized frequency division multiplexing (GFDM) [7] is one of the prominent non-CP-OFDM-based waveforms. It has recently attracted significant attention from the researchers because of its beneficial properties to fulfill the requirements of future wireless networks. A GFDM symbol consists KM samples where each of K subcarriers carry M timeslots. These parameters can be tuned to match the requirements of the application. Consequently, GFDM has a flexibility to engineer the time-frequency structure according to corresponding scenario. In GFDM, each subcarrier is filtered using circular convolution. Therefore, OOB emission of GFDM is considerably low and it can serve for fragmented and opportunistic spectrum allocation purposes. GFDM uses a single CP for an entire block that contains multiple sub-symbols. This enables frequency domain equalization (FDE) and improves the spectral efficiency. Thus, flexible characteristics of GFDM can be easily tuned to address the new requirements.

Multiple-input multiple-output (MIMO)-friendliness is a key ability for a physical layer scheme to satisfactorily match the foreseen requirements of future wireless networks. Since GFDM is a generalized form of OFDM, one can expect that its combination with MIMO is feasible. This was shown for space-time coding (STC) technique [7]–[10] and spatial multiplexing [11]–[17]. In [11] and [12], iterative MIMO decoders have been evaluated. In [13], separate detection and demodulation (SDD) with minimum mean squared error (MMSE) detector and zero-forcing (ZF) GFDM demodulation was proposed. In [14], an equivalent MIMO-GFDM channel model, which combines GFDM modulation and MIMO channel, has been presented and sphere decoding (SD) of subcarrier groups with successive interference cancellation (SIC) was proposed. Based on this equivalent MIMO channel model, MMSE with parallel interference cancellation (MMSE-PIC) detector was proposed in [15] and coded performance analysis of MIMO-GFDM system was performed in [16]. In [17], a low complexity implementation of MMSE equalization was proposed and link level performance of MIMO-GFDM was analyzed along with the CP-OFDM-based counterparts. Nevertheless, when spatial multiplexing is employed with GFDM, inter-antenna interference (IAI) is added to inherent self-interference of GFDM and makes the receiver design challenging.

The continuing demand for higher data rates motivates the researchers to seek spectrally efficient new modulation schemes. Spatial modulation (SM) is a MIMO transmission method, which considers the transmit antennas as spatial constellation points to carry additional information bits [18]. In SM, at each time interval, a single transmit antenna is activated by the input bit sequences and other antennas remain silent. For SM multicarrier schemes, only one transmit antenna is activated at any subcarrier. As a result, activating single transmit antenna at a time or subcarrier eliminates IAI and reduces the receiver complexity. Moreover, SM techniques are more robust to channel imperfections and enhance the error performance.

SM-based modulation schemes have recently received a great deal of interest due to their attractive advantages over classical MIMO systems. Space-shift keying (SSK) is a special case of SM, where only active transmit antenna indices are used to convey information. In SSK, phase shift keying (PSK)/quadrature amplitude modulation (QAM) symbols are not used and active transmit antenna transmits a fixed non-data bearing signal. Space-time shift keying (STSK) is another SM-based modulation scheme, where both the indices of multiple pre-assigned dispersion matrices and signal constellation points are used to convey information. Additionally, the concept of SM is extended to include both the space and time dimensions. Quadrature SM (QSM) [19] expands the spatial constellation symbols to in-phase and quadrature components, and doubles the number of spatially carried bits with respect to a conventional SM system. In QSM, signal constellation symbol is divided into its real and imaginary parts and their corresponding transmit antennas are determined by the input bit sequences in a separate fashion. It is demonstrated that QSM achieves the same error performance and spectral efficiency using 3 dB less signal power with respect to its SM counterpart without increasing the receiver complexity [19].

OFDM with index modulation (IM) is an extension of spatial modulation concept to subcarrier indices in multicarrier systems [20]–[22]. In OFDM-IM, active subcarriers are selected by the input bit sequences and the information bits are conveyed through both the activated subcarrier indices and the conventional modulation symbols. While OFDM-IM scheme improves the error performance by conveying extra information through active subcarrier indices, it reduces throughput due to unused subcarriers. In [23], a dual-mode (DM) OFDM-IM (DM-OFDM) scheme has been proposed to prevent throughput loss still using subcarrier indices to convey extra information. In DM-OFDM scheme, based on the OFDM subblocks concept in [20],

two different constellation modes have been used to modulate the subcarriers with selected indices and the remaining subcarriers. More recently, a multiple-mode DM-OFDM scheme is proposed in [24] by considering full permutation of modes. In order to improve the spectral efficiency, diversity and coding gains of OFDM-IM, several studies have been also performed in recent times [25]–[29]. Furthermore, in [30]–[33], combination of the OFDM-IM technique with MIMO methods has been investigated and significant performance gains have been reported. For a comprehensive overview of OFDM-IM and related literature, interested readers are referred to [34].

Although 3GPP embraces a non-backward compatible radio access technology (RAT) for 5G [35], it is expected that 5G new radio (NR) will be based on CP-OFDM-based waveforms along with the multiple OFDM numerologies due to complexity, latency and maturity issues of non-CP-OFDM-based waveforms. However, considering the continuing massive growth trend in number of wireless devices and applications, the sufficiency of CP-OFDM-based NR is quite disputable. Thus, research efforts on the novel RATs including advanced waveforms and more flexible radio accessing schemes must continue for future wireless networks. In this context, more advanced parameterization schemes in numerology design, e.g., numerology with new parameters such as windowing and user-specific filters, and novel frame design principles, e.g., frame design with multiple base waveforms, are proposed in [36]. In addition to these proposals, non-CP-OFDM-based waveforms along with the promising schemes, such as IM, are one of the prominent concepts to enhance the RAT flexibility.

Non-CP-OFDM-based waveform proposals suffer from self-introduced interference, which eventually results much increased receiver complexity especially for MIMO transmission due to additional IAI. Keeping mind the appealing advantages of the IM concept over classical OFDM, such as flexible system design with adjustable number of active subcarriers, improved error performance for low-to-mid spectral efficiencies and simple transceiver design, we believe that tight integration of GFDM with the IM concept has a strong potential to fulfill the foreseen requirements of future wireless networks in a satisfactory manner. In this context, the application of the SM-GFDM system has been considered in [37], where due to the use of a suboptimal receiver, a poor error performance has been obtained. In addition, the combination of the IM technique [38] with GFDM has been investigated in [39], where a throughput loss was obtained due to the unused subcarriers. Furthermore, combination of GFDM with SM and IM techniques, namely space and frequency IM (SFIM), has been investigated in [40] and significant performance gains have been achieved at the expense of increased computational complexity. As a result, the existing studies on the integration of GFDM with promising IM techniques are not satisfactory to improve the spectral efficiency as well as the error performance and computational complexity at the same time.

In this paper, a framework that comprise the existing studies on the combination of GFDM with IM concept is presented and integration of GFDM with IM concept is discussed in detail to pave the way for innovative transceiver structures. Then, by using this framework, novel transmitter and receiver schemes for MIMO-GFDM applications are proposed. Bit error ratio (BER) performances of the proposed schemes are compared and their computational complexities and spectral efficiencies are analyzed. Based on the obtained results, a guideline for selecting the proper MIMO-GFDM scheme considering target performance criterion is given. The contributions of this paper can be summarized as follows:

- A GFDM-based flexible IM (FIM) transceiver, which is capable of generating and decoding various IM schemes, is proposed. Thanks to FIM, switching between different IM schemes to adapt the channel conditions can be possible using a single transceiver structure.
- FIM provides a multilayer transmission scheme by effectively using space, frequency, and time dimensions to adjust the BER performance and spectral efficiency, and enables to support different use-cases by using common space, frequency, and time resources at the same time.
- A novel QSM-based GFDM scheme is proposed as a special case of FIM to enhance the spectral efficiency while preserving the advantages of SM. To the best of our knowledge, this contribution would be the first approach that exploits multicarrier transmission for QSM. In addition, QSM transmission is combined with the SFIM scheme.
- A near-optimum detection scheme, which is based on maximum likelihood (ML) detection with SIC, is proposed.
- It is shown that ML-SIC detection scheme is also applicable for single-input single-output (SISO), SM, IM, SFIM, and SSK-based GFDM systems.

The remaining sections are organized as follows. The system models of the GFDM-FIM transmitter and receiver are presented in Section II and Section III, respectively. In Sections IV and V, computational complexity and spectral efficiency of the proposed GFDM-FIM schemes are analyzed. Numerical results about the BER performance, computational complexity and spectral efficiency of the proposed GFDM-FIM schemes are presented in Section VI and discussed in Section VII. Finally, Section VIII concludes the paper.[1]

[1] *Notation*: Vectors and matrices are denoted by boldface lowercase and capital letters, respectively. $(\cdot)^T$ and $(\cdot)^H$ denote transposition and Hermitian transposition of a vector or a matrix, respectively, and $(\cdot)^{-1}$ indicates the inverse of a matrix. $C(u, v)$ denotes the binomial coefficient and $\lfloor \cdot \rfloor$ is the floor function. $X \sim \mathcal{CN}(0, \sigma_X^2)$ represents the distribution of a circularly symmetric complex Gaussian random variable X with variance σ_X^2. $\Re\{X\}$ and $\Im\{X\}$ denote the real and imaginary parts of a complex variable X, respectively. diag$(\cdot)$ denotes a diagonal matrix and $\|\cdot\|$ stands for the Euclidean norm. $\mathcal{S}$ denotes Q-ary signal constellation and $\mathbf{x}(a : b)$ stands for all elements of $\mathbf{x}$ between ath and bth indices, inclusive of a and b.

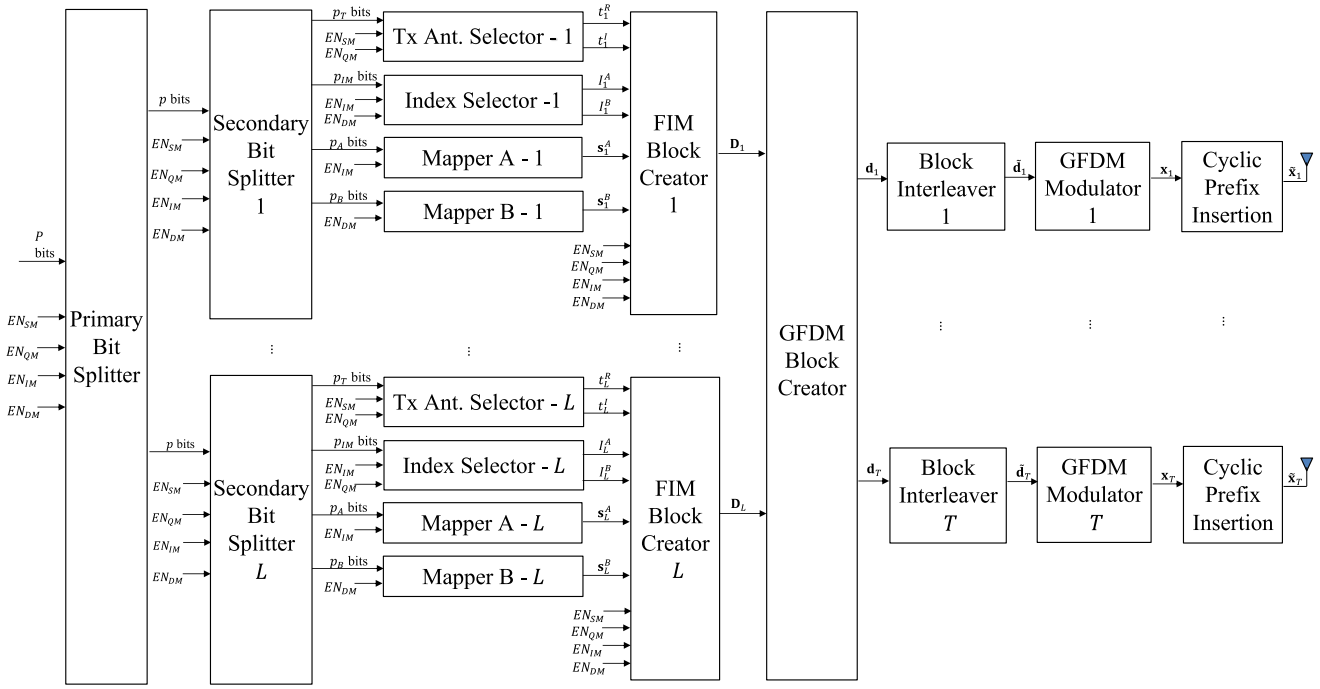

FIGURE 1. Block diagram of the GFDM-FIM transmitter.

TABLE 1. System parameters.

Description	*Parameter*
Number of transmit antennas	T
Number of receive antennas	R
Number of subcarriers in a GFDM subsymbol	K
Number of GFDM subsymbols	M
Total number of subcarriers in a GFDM symbol	N
SM control signal	EN_{SM}
QSM control signal	EN_{QM}
IM control signal	EN_{IM}
Dual Mode IM control signal	EN_{DM}
Number of subcarriers in a subcarrier IM group	u
Number of subcarriers in a primary IM subgroup	v
Number of subcarriers in a secondary IM subgroup	$u-v$
Number of IM subcarrier groups	L
Number of symbols in primary symbol constellation	Q_A
Number of symbols in secondary symbol constellation	Q_B

TABLE 2. Flexible IM control table.

Scheme	EN_{SM}	EN_{QM}	EN_{IM}	EN_{DM}
GFDM	0	0	0	0
GFDM-IM	0	0	1	0
GFDM-DMIM	0	0	1	1
SM-GFDM	1	0	0	0
QSM-GFDM	1	1	0	0
SFIM-GFDM	1	0	1	0
QSFIM-GFDM	1	1	1	0
SFDMIM-GFDM	1	0	1	1
QSFDMIM-GFDM	1	1	1	1

II. GFDM-FIM TRANSMITTER

As mentioned earlier, GFDM has a block structure consisting of $N = KM$ samples where K subcarriers constitute a GFDM subsymbol and M GFDM subsymbols constitute a GFDM symbol. In this study, a MIMO-GFDM system with T transmit and R receive antennas is considered. The system has four control signals named as EN_{SM}, EN_{QM}, EN_{IM}, and EN_{DM}, which control SM, QSM, IM, and dual mode IM (DMIM) operation modes, respectively, in an on/off fashion, where EN_{SM}, EN_{QM}, EN_{IM}, $EN_{DM} \in \{0, 1\}$. The overall system parameters are given in Table 1. Specific implementations of SM and IM schemes with respect to control signals are given in Table 2. Thanks to these control signals, existing schemes, such as, GFDM-based IM, DMIM, SM, and SFIM and new SM and IM schemes, such as, GFDM based QSM, space and frequency DMIM (SFDMIM), quadrature SFIM (QSFIM) and quadrature SFDMIM (QSFDMIM) can be implemented by using a single transmitter.

The block diagram of the proposed GFDM-FIM transmitter is given in Fig. 1. Primary bit splitter block accepts P data bits from the input bit stream along with the control signals and splits these P bits into L groups with p bits, i.e., $p = P/L$. Then, each group of p bits is mapped to a subcarrier group with u elements in three stages. In this mapping operation, antenna and subcarrier indices as well as Q-ary QAM (Q-QAM) constellations can be used. Besides, constellation symbols can be expanded to in-phase and quadrature components. In order to apply this mapping, secondary bit splitter partitions these p bits into four groups, which contain p_T, p_{IM}, p_A, and p_B bits according to status of the control signals.

The first stage of the mapping is transmit antenna selection. At this stage, Tx antenna selector block gets

$$p_T = EN_{SM}(1 + EN_{QM}) \log_2(T) \tag{1}$$

bits and selects the indices of the transmit antennas. When both SM and QSM modes are enabled, i.e., $EN_{SM} = 1$, $EN_{QM} = 1$, the first and second $\log_2(T)$-bits parts of the p_T-bit sequence are used to determine the transmit antennas corresponding to the real and the imaginary parts of the vector of the modulated symbols for the subcarrier IM group as t_l^R and t_l^I, respectively, where $t_l^R, t_l^I \in \{1, \ldots, T\}$. When the QSM mode is disabled, i.e., $EN_{QM} = 0$, only t_l^R is determined and it is used as the transmit antenna for both the real and the imaginary parts of the vector of the modulated symbols. Note that when the SM mode is disabled, i.e., $EN_{SM} = 0$, Tx antenna selector block remains inactive and transmission is always realized through a pre-determined transmit antenna.

The second stage of the mapping is index selection. At this stage, when IM mode is enabled, i.e., $EN_{IM} = 1$, index selector blocks gets p_{IM} bits to select the indices of the subcarriers in the primary IM subgroup, denoted as

$$I_l^A = \left\{ i_{l,1}^A, i_{l,2}^A, \ldots, i_{l,v}^A \right\}, \tag{2}$$

where $i_{l,\gamma}^A \in \{1, \ldots, u\}$, for $\gamma = 1, \ldots, v$, and $l \in \{1, \ldots, L\}$. Here, I_l^A is determined to modulate v subcarriers by a selection rule, besides when the DMIM mode is enabled along with the IM mode, i.e., $EN_{DM} = 1$, the remaining $u - v$ subcarriers constitute the indices of the subcarriers in the secondary IM subgroup, denoted as,

$$I_l^B = \left\{ i_{l,1}^B, i_{l,2}^B, \ldots, i_{l,u-v}^B \right\}, \tag{3}$$

where $i_{l,\gamma}^B \in \{1, \ldots, u\}$, for $\gamma = 1, \ldots, u - v$ and $l \in \{1, \ldots, L\}$. Since I_l^A has $c = 2^{p_{IM}}$ possible realizations, only c out of $C(u, v)$ possible combinations are used. Therefore, p_{IM} can be defined as

$$p_{IM} = EN_{IM} \lfloor \log_2 (C(u, v)) \rfloor. \tag{4}$$

Note that when the IM mode is disabled, i.e., $EN_{IM} = 0$, index selector block remains inactive and all subcarriers are used without any selection.

The third stage of the mapping is QAM modulation. At this stage, mapper A gets p_A bits to modulate the subcarriers selected by I_l^A and uses constellation set of $\mathcal{S}^A$, which has Q_A elements, to modulate v subcarriers. Therefore, p_A can be defined as

$$p_A = v \log_2(Q_A). \tag{5}$$

When the DMIM mode is enabled along with the IM mode, i.e., $EN_{DM} = 1$, mapper B gets p_B bits to modulate the subcarriers selected by I_l^B and uses constellation set of $\mathcal{S}^B$, which has Q_B elements, to modulate $u - v$ subcarriers. Therefore, p_B can be defined as

$$p_B = EN_{IM} EN_{DM} (u - v) \log_2(Q_B). \tag{6}$$

At this point, in order to reliably detect the subcarrier index subgroups at the receiver, the constellations used by the mappers A and B have to be disjoint sets, i.e., $\mathcal{S}^A \cap \mathcal{S}^B = \varnothing$. As a result, the vector of the modulated symbols mapped by mapper A for the index subgroup I_l^A, which carries p_A bits, and the vector of the modulated symbols mapped by mapper B for the index subgroup I_l^B, which carries p_B bits, can be expressed by

$$\mathbf{s}_l^A = \left[s_l^A(1), s_l^A(2), \ldots, s_l^A(v) \right]^T, \tag{7}$$

$$\mathbf{s}_l^B = \left[s_l^B(1), s_l^B(2), \ldots, s_l^B(u - v) \right]^T, \tag{8}$$

where $s_l^A(\gamma) \in \mathcal{S}^A$, for $\gamma = 1, \ldots, v$, $s_l^B(\gamma) \in \mathcal{S}^B$, for $\gamma = 1, \ldots, u - v$, respectively. Note that, when the IM mode is disabled, i.e., $EN_{IM} = 0$, both u and v are equal to 1 and $\mathbf{s}_l^A$ contains one Q-ary symbol and $\mathbf{s}_l^B$ is a null vector. Then, FIM block creator combines $\mathbf{s}_l^A$ and $\mathbf{s}_l^B$ and creates the vector of the modulated symbols for the subcarrier group l as

$$\mathbf{s}_l = [s_l(1), s_l(2), \ldots, s_l(u)]^T, \tag{9}$$

where $\mathbf{s}_l(\gamma) \in \left\{ \mathcal{S}^A, \mathcal{S}^B, 0 \right\}$, for $\gamma = 1, \ldots, u$. After that, transmit antenna assignment procedure is executed according to status of the control signal EN_{QM}. When the QSM mode is enabled, i.e., $EN_{QM} = 1$, the in-phase parts of $\mathbf{s}_l$ are assigned to antenna t_l^R and the quadrature parts of the $\mathbf{s}_l$ are assigned to antenna t_l^I as

$$\mathbf{s}_{t_l^R,l} = \left[s_{t_l^R,l}(1), s_{t_l^R,l}(2), \ldots, s_{t_l^R,l}(u) \right]^T, \tag{10}$$

$$\mathbf{s}_{t_l^I,l} = \left[s_{t_l^I,l}(1), s_{t_l^I,l}(2), \ldots, s_{t_l^I,l}(u) \right]^T, \tag{11}$$

where $s_{t_l^R,l}(\gamma) \in \left\{ \Re\{\mathcal{S}^A\}, \Re\{\mathcal{S}^B\}, 0 \right\}$, for $t_l^R \in \{1, \ldots, T\}$, $s_{t_l^I,l}(\gamma) \in \left\{ \Im\{\mathcal{S}^A\}, \Im\{\mathcal{S}^B\}, 0 \right\}$, for $t_l^I \in \{1, \ldots, T\}$, $\gamma = 1, \ldots, u$. On the other hand, when the QSM mode is disabled, i.e., $EN_{QM} = 0$, both the in-phase and quadrature parts of $\mathbf{s}_l$ are assigned to transmit antenna t_l^R, i.e., $s_{t_l^R,l}(\gamma) \in \left\{ \mathcal{S}^A, \mathcal{S}^B, 0 \right\}$ and $\mathbf{s}_{t_l^I,l}$ is a null vector. Afterwards, FIM block creator sets the subcarriers of the inactive antennas to zero and arranges the transmit symbols for block l in a $T \times u$ matrix $\mathbf{D}_l$, where t_l^Rth row of $\mathbf{D}_l$ is $\mathbf{s}_{t_l^R,l}$ and t_l^Ith row of $\mathbf{D}_l$ is $\mathbf{s}_{t_l^I,l}$. Then, GFDM block creator combines the FIM blocks and we obtain

$$\mathbf{D} = [\mathbf{D}_1, \mathbf{D}_2, \ldots, \mathbf{D}_L], \tag{12}$$

where $\mathbf{D}$ is a $T \times N$ matrix. As a result, the GFDM symbol for the transmit antenna t, which is tth row vector of $\mathbf{D}$, can be expressed by

$$\mathbf{d}_t = \left[d_{t,0,0}, \ldots, d_{t,K-1,0}, d_{t,0,1}, \ldots, d_{t,K-1,1}, \ldots, d_{t,K-1,M-1} \right], \tag{13}$$

where $d_{t,k,m}$ is the data symbol of mth timeslot on kth subcarrier belonging to tth antenna. In [32] and [39], a block interleaver is used to render the channel memoryless; therefore, when the IM mode is active, i.e., $EN_{IM} = 1$, $L \times u$ block interleaving is applied to $\mathbf{d}_t$ and the interleaved data vector $\widetilde{\mathbf{d}}_t$ is obtained. After block interleaving, $\widetilde{\mathbf{d}}_t$ is modulated using a GFDM modulator and the overall GFDM transmit signal $x_t(n)$ of tth transmit antenna is given by

$$x_t(n) = \sum_{k=0}^{K-1} \sum_{m=0}^{M-1} \widetilde{d}_{t,k,m} g_{k,m}(n), \tag{14}$$

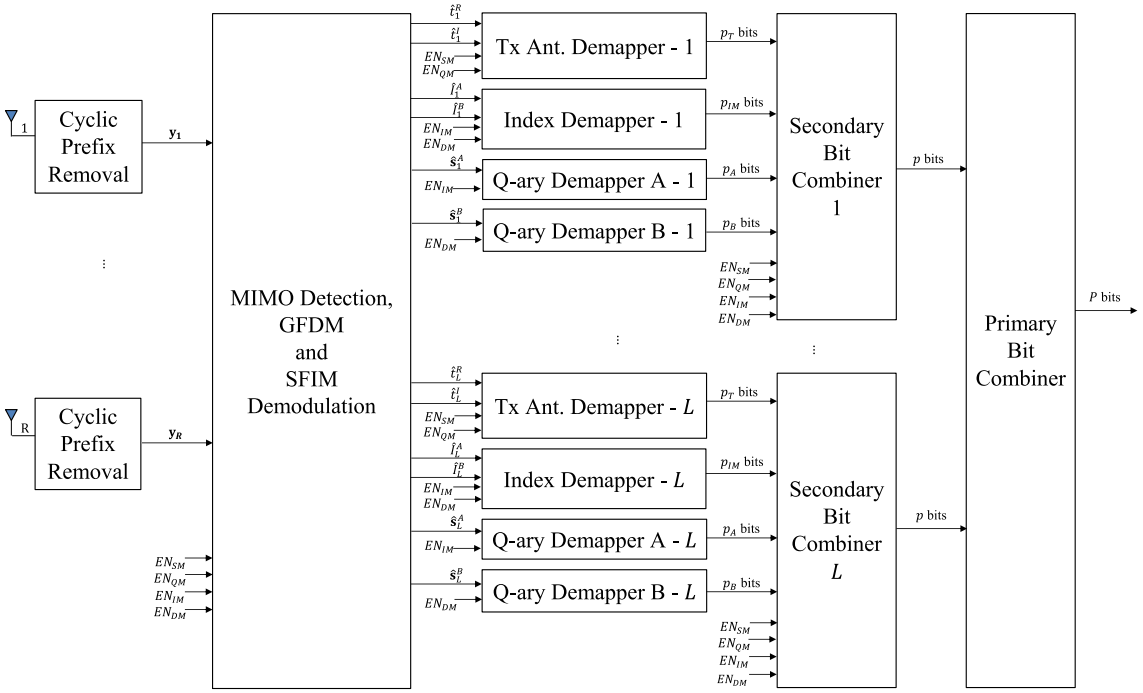

FIGURE 2. Block diagram of the GFDM-FIM receiver.

where $n \in \{0, \ldots, N-1\}$ denotes the sampling index and

$$g_{k,m}(n) = g\left((n - mK)_{\text{mod}N}\right) \exp\left(j2\pi \frac{kn}{K}\right) \tag{15}$$

is the transmit filter circularly shifted to the mth timeslot and modulated to the kth subcarrier. After collecting the filter samples in a vector $\mathbf{g}_{k,m} = \left[g_{k,m}(0), \ldots, g_{k,m}(N-1)\right]^T$, (14) can be rewritten as

$$\mathbf{x}_t = \mathbf{A}\widetilde{\mathbf{d}}_t, \tag{16}$$

where $\mathbf{A}$ is a $KM \times KM$ transmitter matrix [7] with the following structure:

$$\mathbf{A} = \left[\mathbf{g}_{0,0}, \ldots, \mathbf{g}_{K-1,0}, \mathbf{g}_{0,1}, \ldots, \mathbf{g}_{K-1,1}, \ldots, \mathbf{g}_{K-1,M-1}\right]. \tag{17}$$

The last step at the transmitter side is the addition of a CP with length N_{CP} in order to make the convolution with the channel circular and the resulting vector

$$\tilde{\mathbf{x}}_t = \left[\mathbf{x}_t\left(KM - N_{\text{CP}} + 1 : KM\right)^T, \mathbf{x}_t^T\right]^T \tag{18}$$

is obtained. Finally, $\tilde{\mathbf{x}}_t$ is transmitted over a frequency-selective Rayleigh fading channel.

III. GFDM-FIM RECEIVER

The block diagram of the proposed GFDM-FIM receiver is given in Fig. 2. After the removal of CP, assuming that the wireless channel remains constant during the transmission of a GFDM block, CP is longer than the tap length of the channel (N_{Ch}) and perfect synchronization is ensured, the overall received signal can be expressed as

$$\begin{bmatrix}\mathbf{y}_1\\ \vdots \\ \mathbf{y}_R\end{bmatrix} = \begin{bmatrix}\mathbf{H}_{1,1} & \cdots & \mathbf{H}_{1,T}\\ \vdots & \ddots & \vdots \\ \mathbf{H}_{R,1} & \cdots & \mathbf{H}_{R,T}\end{bmatrix}\begin{bmatrix}\mathbf{x}_1\\ \vdots \\ \mathbf{x}_T\end{bmatrix} + \begin{bmatrix}\mathbf{w}_1\\ \vdots \\ \mathbf{w}_R\end{bmatrix}, \tag{19}$$

where $\mathbf{y}_r = [y_r(0), y_r(1), \ldots, y_r(N-1)]^T$ is the vector of received signals at the rth receive antenna, $\mathbf{H}_{r,t}$, for $t = 1, \ldots, T$, $r = 1, \ldots, R$, is the $N \times N$ circular convolution matrix constructed from the channel impulse response coefficients between the tth transmit antenna and the rth receive antenna given by $\mathbf{h}_{r,t} = \left[h_{r,t}(0), h_{r,t}(1), \ldots, h_{r,t}(N_{\text{Ch}}-1)\right]^{\text{T}}$, where $h_{r,t}(n)$ follows $\mathcal{CN}(0, 1)$ distribution, $\mathbf{w}_r$ is an $N \times 1$ vector of additive white Gaussian noise (AWGN) samples with elements distributed as $\mathcal{CN}(0, \sigma_w^2)$. After substituting (16) in (19), we obtain

$$\begin{bmatrix}\mathbf{y}_1\\ \vdots \\ \mathbf{y}_R\end{bmatrix} = \begin{bmatrix}\mathbf{H}_{1,1}\mathbf{A} & \cdots & \mathbf{H}_{1,T}\mathbf{A}\\ \vdots & \ddots & \vdots \\ \mathbf{H}_{R,1}\mathbf{A} & \cdots & \mathbf{H}_{R,T}\mathbf{A}\end{bmatrix}\begin{bmatrix}\widetilde{\mathbf{d}}_1\\ \vdots \\ \widetilde{\mathbf{d}}_T\end{bmatrix} + \begin{bmatrix}\mathbf{w}_1\\ \vdots \\ \mathbf{w}_R\end{bmatrix}. \tag{20}$$

(20) can be rewritten in a more compact form as

$$\mathbf{y} = \widetilde{\mathbf{H}}\widetilde{\mathbf{d}} + \mathbf{w}, \tag{21}$$

where the dimensions of $\mathbf{y}$, $\widetilde{\mathbf{H}}$, $\widetilde{\mathbf{d}}$ and $\mathbf{w}$ are $NR \times 1$, $NR \times NT$, $NT \times 1$ and $NR \times 1$, respectively. The most critical part of the GFDM-FIM receiver is the block of MIMO detection, GFDM and SFIM demodulation. For MIMO-OFDM, MIMO detection and SFIM demodulation can be performed at the subcarrier level due to orthogonality in the frequency domain.

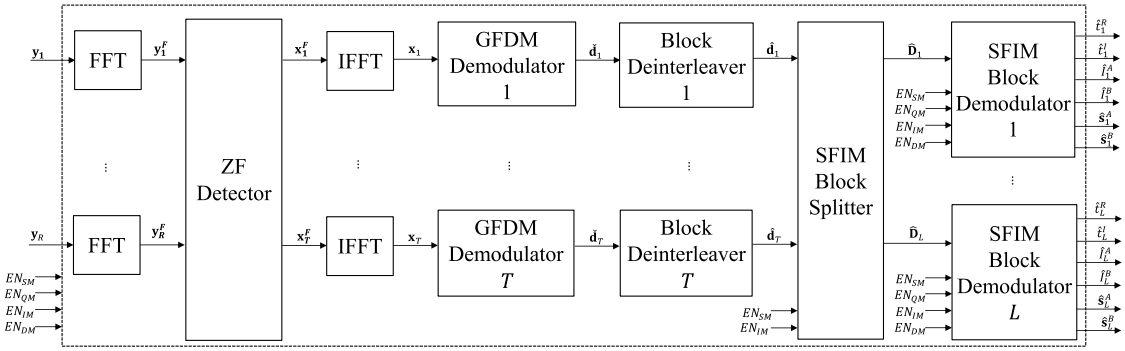

FIGURE 3. Block diagram of the ZF-SDD based separate MIMO detection, GFDM and SFIM demodulation.

In GFDM, the inherent intercarrier interference (ICI) prevents the frequency domain decoupling of GFDM subcarriers for both SISO and MIMO transmission schemes. In [37], MIMO detection, GFDM demodulation and spatial demodulation are treated independently, where a poor error performance has been obtained. In [39], GFDM demodulation and index demodulation are handled as two distinct tasks. In [40], while joint MIMO detection and GFDM demodulation has been proposed, SFIM demodulation has been treated in an independent way. As will be shown later, these methods are also applicable for the GFDM-FIM receiver. Besides, in this paper, a new method is proposed by treating MIMO detection, GFDM and SFIM demodulation jointly. These methods will be presented as three alternatives for MIMO detection, GFDM and SFIM demodulation block of the GFDM-FIM receiver in the subsequent subsections.

After MIMO detection, GFDM and SFIM demodulation, the information bits are recovered by applying the inverse mapping process for both modulated symbols and indices of the active transmit antennas and subcarriers. Then, the secondary bit combiner combines the outputs of the demappers and forms the p-bit sequence, which is the estimate of the input of the secondary bit splitter. Finally, the primary bit combiner combines all p-bit groups and forms the original P-bit data sequence.

A. ZF-SDD BASED SEPARATE MIMO DETECTION, GFDM AND SFIM DEMODULATION

The block diagram of the proposed ZF-SDD Based Separate MIMO Detection, GFDM and SFIM Demodulation method is given in Fig. 3. Based on the system model of (19), after performing fast Fourier transform (FFT) operations in each antenna branch of the receiver, the input-output relationship of the GFDM-FIM scheme in the frequency domain is obtained as

$$\mathbf{y}_r^F = \sum_{t=1}^{T} \text{diag}(\mathbf{x}_t^F)\mathbf{h}_{r,t}^F + \mathbf{w}_r^F, \tag{22}$$

where $\mathbf{y}_r^F = [y_r^F(0), y_r^F(1), \ldots, y_r^F(N-1)]^T$ is the vector of received signals at the rth receive antenna, for $r = 1, \ldots, R$, and $\mathbf{h}_{r,t}^F = \left[h_{r,t}^F(0), h_{r,t}^F(1), \ldots, h_{r,t}^F(N-1)\right]^{\mathrm{T}}$ is the frequency response of the wireless channel between the transmit antenna t and receive antenna r, where $h_{r,t}^F(\gamma)$ follows $\mathcal{CN}(0, 1)$ distribution, $\mathbf{w}_r^F$ is an $N \times 1$ vector of noise samples distributed as $\mathcal{CN}(0, \sigma_w^2)$. Since GFDM block is made up of KM subcarriers, the following signal model is obtained from (22) for kth subcarrier of mth subsymbol:

$$\begin{bmatrix} y_1^F(k,m) \\ y_2^F(k,m) \\ \vdots \\ y_R^F(k,m) \end{bmatrix} = \begin{bmatrix} h_{1,1}^F(k,m) & \cdots & h_{1,T}^F(k,m) \\ h_{2,1}^F(k,m) & \cdots & h_{2,T}^F(k,m) \\ \vdots & \ddots & \vdots \\ h_{R,1}^F(k,m) & \cdots & h_{R,T}^F(k,m) \end{bmatrix} \begin{bmatrix} x_1^F(k,m) \\ x_2^F(k,m) \\ \vdots \\ x_T^F(k,m) \end{bmatrix} + \begin{bmatrix} w_1^F(k,m) \\ w_2^F(k,m) \\ \vdots \\ w_R^F(k,m) \end{bmatrix}. \tag{23}$$

(23) can be rewritten in a more compact form as

$$\mathbf{y}_{k,m}^F = \mathbf{H}_{k,m}^F \mathbf{x}_{k,m}^F + \mathbf{w}_{k,m}^F, \tag{24}$$

where $\mathbf{y}_{k,m}^F$ is the received signal vector, $\mathbf{H}_{k,m}^F$, for $k = 0, \ldots, K-1$, $m = 0, \ldots, M-1$, is the $R \times T$ corresponding channel matrix that contains the channel coefficients between transmit and receive antennas and assumed to be perfectly known at the receiver, $\mathbf{x}_{k,m}^F$ is the data vector, which contains the simultaneously transmitted symbols from all transmit antennas and $\mathbf{w}_{k,m}^F$ is the noise vector. Here, an estimate of $\mathbf{x}_{k,m}^F$ can be obtained by using ZF detection approach as follows:

$$\widehat{\mathbf{x}}_{k,m}^F = \left(\mathbf{H}_{k,m}^F\right)^{-1} \mathbf{y}_{k,m}^F. \tag{25}$$

Rearranging of vectors $\widehat{\mathbf{x}}_{k,m}^F$ as column vectors of a matrix gives

$$\widehat{\mathbf{X}}^F = \left[(\widehat{\mathbf{x}}_{0,0}^F)^T, \ldots, (\widehat{\mathbf{x}}_{K-1,0}^F)^T, (\widehat{\mathbf{x}}_{0,1}^F)^T, \ldots, (\widehat{\mathbf{x}}_{K-1,M-1}^F)^T\right], \tag{26}$$

where each row contains an estimate of the frequency domain representation of the transmit vector for the corresponding

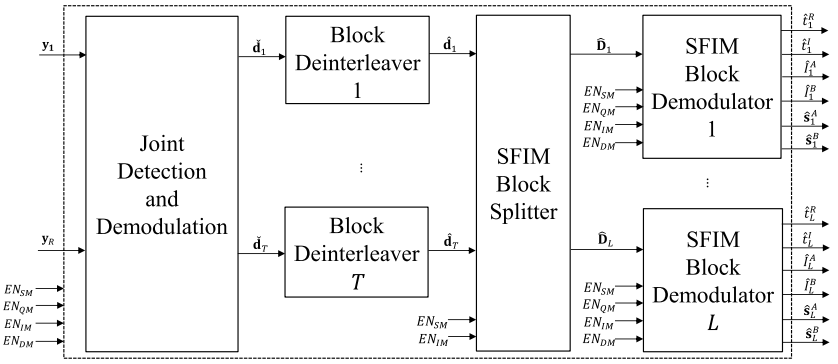

FIGURE 4. Block diagram of the MMSE-JDD based joint MIMO detection and GFDM demodulation, separate SFIM demodulation.

antenna, that is:

$$\widehat{\mathbf{X}}^F = \begin{bmatrix} \widehat{\mathbf{x}}_1^F \\ \widehat{\mathbf{x}}_2^F \\ \vdots \\ \widehat{\mathbf{x}}_T^F \end{bmatrix}. \tag{27}$$

Then, inverse FFT (IFFT) of size N is applied to $\widehat{\mathbf{x}}_t^F$ and $\widehat{\mathbf{x}}_t$ is obtained. Afterwards, linear GFDM demodulation of the $\widehat{\mathbf{x}}_t$ is obtained by using ZF approach:

$$\breve{\mathbf{d}}_t = \mathbf{A}^{-1}\widehat{\mathbf{x}}_t \tag{28}$$

After this point, if block interleaving was applied at the transmitter, $L \times u$ block deinterleaving is applied to $\breve{\mathbf{d}}_t$ and $\widehat{\mathbf{d}}_t$ is obtained. SFIM block splitter partitions $\widehat{\mathbf{d}}_t$ into L groups with length u and arranges these groups in a $T \times u$ matrix given by

$$\widehat{\mathbf{D}}_l = \begin{bmatrix} \widehat{\mathbf{s}}_{1,l} \\ \vdots \\ \widehat{\mathbf{s}}_{T,l} \end{bmatrix} = \begin{bmatrix} \widehat{\mathbf{d}}_1((l-1)u+1:lu) \\ \vdots \\ \widehat{\mathbf{d}}_T((l-1)u+1:lu) \end{bmatrix}. \tag{29}$$

Note that when the IM mode is disabled, i.e., $EN_{IM} = 0$, u is equal to 1 and $\widehat{\mathbf{s}}_{t,l}$, for $t = 1, \ldots, T$, has only one element. Then, SFIM block demodulator makes a joint decision on the indices of transmit antennas corresponding to the in-phase and the quadrature parts of the vector of the modulated symbols, subcarrier index subgroups as well as constellation symbols considering all possible realizations of $\mathbf{D}_l$ by minimizing the following metric:

$$\left\{\hat{t}_l^R, \hat{t}_l^I, \hat{I}_l^A, \hat{\mathbf{s}}_l^A, \hat{\mathbf{s}}_l^B\right\} = \underset{t, I^A, \mathcal{S}^A, \mathcal{S}^B}{\arg\min} \|\widehat{\mathbf{D}}_l - \mathbf{D}_l\|_F^2. \tag{30}$$

B. MMSE BASED JOINT MIMO DETECTION AND GFDM DEMODULATION, SEPARATE SFIM DEMODULATION

The block diagram of the proposed MMSE Based Joint MIMO Detection and GFDM Demodulation, Separate SFIM Demodulation method is given in Fig. 4. Thanks to system model of (21), unlike ZF-SDD based MIMO detection, GFDM and SFIM demodulation, which uses zero-forcing (ZF) detector in the frequency domain, thus, handles MIMO detection and GFDM demodulation separately, GFDM modulation and MIMO channel can be linearly modeled. As a result, joint MIMO detection and GFDM demodulation (JDD) through MMSE filtering can be performed by

$$\breve{\mathbf{D}} = \left(\widetilde{\mathbf{H}}^{\mathrm{H}}\widetilde{\mathbf{H}} + \sigma_w^2\mathbf{I}\right)^{-1}\widetilde{\mathbf{H}}^{\mathrm{H}}\mathbf{y}, \tag{31}$$

where tth row of $\breve{\mathbf{D}}$ is $\breve{\mathbf{d}}_t$, which is the estimation of the output of the tth block interleaver. Then, block deinterleaving, SFIM block splitting and SFIM block demodulation are performed as explained in Section III-A.

C. ML-SIC BASED JOINT MIMO DETECTION, GFDM AND SFIM DEMODULATION

The block diagram of the proposed ML-SIC Based Joint MIMO Detection, GFDM and SFIM Demodulation method is given in Fig. 5. In GFDM, as mentioned earlier, the inherent ICI prevents the frequency domain decoupling of GFDM subcarriers for both SISO and MIMO transmission schemes; therefore, simultaneous detection of all subcarriers is required for optimum decision. Since this process is computationally infeasible, low complexity solutions are required for the optimum detection problem of MIMO-GFDM. In [14], an algorithm including SD of subcarrier groups with SIC is proposed for spatial multiplexing. By properly organizing the columns of $\widetilde{\mathbf{H}}$ in (21), the algorithm in [14] can be modified to jointly detect the antenna and subcarrier indices as well as the transmitted symbols for GFDM-FIM schemes. The QR-decomposition [41] of the channel matrix $\widetilde{\mathbf{H}}$ is given as

$$\widetilde{\mathbf{H}} = \mathbf{QRP}^{\mathrm{T}}, \tag{32}$$

where $\mathbf{Q}$ is an $NR \times NT$ unitary matrix, $\mathbf{R}$ is an $NT \times NT$ upper triangular matrix, and $\mathbf{P}$ sorts the columns of $\widetilde{\mathbf{H}}$ prior to decomposition to detect the transmitted symbols at the SFIM block level. Note that if block interleaving was applied at the transmitter, block deinterleaving must be applied to the columns of $\widetilde{\mathbf{H}}$ prior to sorting. The QR decomposer combines the received signals, i.e., $\mathbf{y} = \left[\mathbf{y}_1{}^{\mathrm{T}}, \mathbf{y}_2{}^{\mathrm{T}}, \ldots, \mathbf{y}_R{}^{\mathrm{T}}\right]^{\mathrm{T}}$,

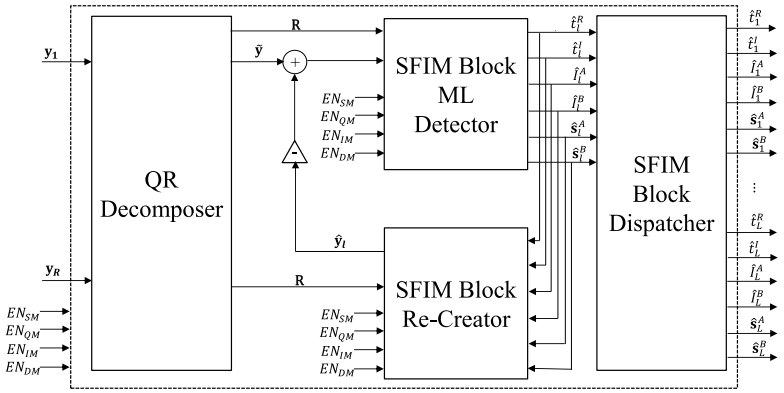

FIGURE 5. Block diagram of the ML-SIC based joint MIMO detection, GFDM and SFIM demodulation.

TABLE 3. Computational complexity of ZF-SDD based GFDM-FIM receiver.

Process	*Scheme*	*Operation*	*Execution Count*	*Complexity (CMs)*
DFT block	all	$\mathrm{DFT}(\phi_{N\times 1})^*$	R	N^2R
ZF detection	all	$(\Phi_{R\times T})^+\phi_{R\times 1}$	N	$2NT^2R + NT^3 + NTR$
IDFT block	all	$\mathrm{IDFT}(\phi_{N\times 1})^*$	T	N^2T
GFDM demod.	all	$\Phi_{N\times N}\phi_{N\times 1}$	T	N^2T
Block Deinter.	all	No CM	R	0
SFIM Demod.	SM	$\min(\|\phi_{T\times 1} - \psi_{T\times 1})\|^2)$	NTQ_A	NT^2Q_A
	QSM	$\min(\|\phi_{T\times 1} - \psi_{T\times 1})\|^2)$	NT^2Q_A	NT^3Q_A
	SFIM	$\min(\|\phi_{T\times u} - \psi_{T\times u})\|^2)$	$(N/u)cQ_A^vT$	$NcQ_A^vT^2$
	QSFIM	$\min(\|\phi_{T\times u} - \psi_{T\times u})\|^2)$	$(N/u)cQ_A^vT^2$	$NcQ_A^vT^3$
	SFDMIM	$\min(\|\phi_{T\times u} - \psi_{T\times u})\|^2)$	$(N/u)cQ_A^vQ_B^{u-v}T$	$NcQ_A^vQ_B^{u-v}T^2$
	QSFDMIM	$\min(\|\phi_{T\times u} - \psi_{T\times u})\|^2)$	$(N/u)cQ_A^vQ_B^{u-v}T^2$	$NcQ_A^vQ_B^{u-v}T^3$

* We consider direct calculation of N-point DFT and IDFT operations, which involve N^2 CMs, since M is odd.

multiplies with $\mathbf{Q}^{\mathrm{H}}$ from the left and obtains the modified received signal vector

$$\tilde{\mathbf{y}} = \mathbf{Q}^{\mathrm{H}}\mathbf{y} = \mathbf{R}\tilde{\mathbf{d}} + \tilde{\mathbf{w}}, \tag{33}$$

where $\tilde{\mathbf{w}} = \mathbf{Q}^{\mathrm{H}}\mathbf{w}$ and

$$\tilde{\mathbf{d}} = \mathbf{P}^{\mathrm{T}}\mathbf{d} = \left[\mathbf{z}_1{}^{\mathrm{T}}, \mathbf{z}_2{}^{\mathrm{T}}, \ldots, \mathbf{z}_L{}^{\mathrm{T}}\right]^{\mathrm{T}}. \tag{34}$$

Here, $\mathbf{z}_l$, for $l = 1, \ldots, L$, is an $uT \times 1$ vector given by

$$\mathbf{z}_l = \left[\mathbf{s}_{1,l}, \mathbf{s}_{2,l}, \ldots, \mathbf{s}_{T,l}\right], \tag{35}$$

where $\mathbf{s}_{t,l}$, for $t = 1, \ldots, T$ and $l \in \{1, \ldots, L\}$, is an $u \times 1$ vector denoted by

$$\mathbf{s}_{t,l} = \left[s_{t,l}(1), s_{t,l}(2), \ldots, s_{t,l}(u)\right] = [\mathbf{d}_t((l-1)u + 1 : lu)]. \tag{36}$$

As stated earlier, when the IM mode is disabled, i.e., $EN_{IM} = 0$, u is equal to 1 and $\widehat{\mathbf{s}}_{t,l}$, for $t = 1, \ldots, T$, has only one element. Then, with the help of the upper triangular structure of $\mathbf{R}$, the SFIM block ML detector finds the ML solution for the last SFIM block, cancels the interference originated from it, reduces the system size by uT and continues to the next SFIM block until all SFIM blocks are detected. The proposed detection algorithm is shown in Algorithm 1. Here,

Algorithm 1 ML-SIC Detection

1: **Input** $= \tilde{\mathbf{y}}, \mathbf{R}$
2: **Output** $= \hat{t}_l^R, \hat{t}_l^I, \hat{I}_l^A, \hat{I}_l^B, \hat{\mathbf{s}}_l^A, \hat{\mathbf{s}}_l^B$ for $l = 1, \ldots, L$
3: **for** $l \leftarrow L$ to 1 **do**
4: $\quad \hat{\mathbf{z}}_l = \underset{t, I^A, \mathcal{S}^A, \mathcal{S}^B}{\operatorname{argmin}} \|\tilde{\mathbf{y}}_{uT} - \mathbf{R}_{uT,uT}\mathbf{z}_l\|^2$
5: $\quad \hat{\mathbf{y}}_l = \mathbf{R}_{:,uT}\hat{\mathbf{z}}_l, \tilde{\mathbf{y}} \leftarrow \tilde{\mathbf{y}} - \hat{\mathbf{y}}_l$
6: $\quad \tilde{\mathbf{y}} \leftarrow \tilde{\mathbf{y}}_{u\bar{T}}, \mathbf{R} \leftarrow \mathbf{R}_{u\bar{T},u\bar{T}}$
7: **end for**

the subscripts uT, $u\bar{T}$ and : denote the last uT, all but the last uT and all elements (column/rows) of the subscripted object, respectively. After this point, for each SFIM block, transmit antennas corresponding to the in-phase and the quadrature parts of the vector of the modulated symbols, subcarrier index subgroups as well as constellation symbols, are estimated as $\hat{t}_l^R, \hat{t}_l^I, \hat{I}_l^A, \hat{I}_l^B, \hat{\mathbf{s}}_l^A, \hat{\mathbf{s}}_l^B$, respectively.

IV. COMPLEXITY ANALYSIS

Computational complexity of four different GFDM-FIM receivers is analyzed in terms of number of complex multiplications (CMs) performed in total and presented in Tables 3, 4, 5 and 6. Here, $\Phi_{J\times I}$ and $\Psi_{J\times I}$ stand for $J \times I$

TABLE 4. Computational complexity of MMSE-JDD based GFDM-FIM receiver.

Process	*Scheme*	*Operation*	*Execution Count*	*Complexity (CMs)*
Forming $\widetilde{\mathbf{H}}$	all	$\Phi_{N\times N}\Psi_{N\times N}{}^{**}$	RT	$N_{\mathrm{Ch}}N^2RT$
JDD	all	$\left(\Phi_{NR\times NT}{}^{\mathrm{H}}\Phi_{NR\times NT}+\Psi_{NT\times NT}\right)^{-1}\Phi_{NR\times NT}{}^{\mathrm{H}}\phi_{NR\times 1}$	1	$2N^3T^2R+N^3T^3+N^2RT$
Block Deinter.	all	No CM	R	0
SFIM Demod.	SM	$\min(\|\phi_{T\times 1}-\psi_{T\times 1})\|^2)$	NTQ_A	NT^2Q_A
	QSM	$\min(\|\phi_{T\times 1}-\psi_{T\times 1})\|^2)$	NT^2Q_A	NT^3Q_A
	SFIM	$\min(\|\phi_{T\times u}-\psi_{T\times u})\|^2)$	$(N/u)cQ_A^vT$	$NcQ_A^vT^2$
	QSFIM	$\min(\|\phi_{T\times u}-\psi_{T\times u})\|^2)$	$(N/u)cQ_A^vT^2$	$NcQ_A^vT^3$
	SFDMIM	$\min(\|\phi_{T\times u}-\psi_{T\times u})\|^2)$	$(N/u)cQ_A^vQ_B^{u-v}T$	$NcQ_A^vQ_B^{u-v}T^2$
	QSFDMIM	$\min(\|\phi_{T\times u}-\psi_{T\times u})\|^2)$	$(N/u)cQ_A^vQ_B^{u-v}T^2$	$NcQ_A^vQ_B^{u-v}T^3$

** In every row of $\mathbf{H}_{r,t}$, which is Φ in this case, only N_{Ch} out of N elements are non-zero.

TABLE 5. Computational complexity of ML-SIC based GFDM-FIM receiver.

Process	*Scheme*	*Operation*	*Execution Count*	*Complexity (CMs)*
Forming $\widetilde{\mathbf{H}}$	all	$\Phi_{N\times N}\Psi_{N\times N}{}^{\dagger}$	RT	$N_{\mathrm{Ch}}N^2RT$
Block Deinter.	all	No CM	R	0
Permutation	all	No CM	1	0
QRD	all	$QR\left(\Phi_{NR\times NT}\right)^{\dagger\dagger}$	1	$2N^3T^2R$
Modified recv. vector	all	$\Phi_{NR\times NT}{}^{\mathrm{H}}\phi_{NR\times 1}$	1	N^2RT
ML Detection	SM	$\min(\|\phi_{T\times 1}-(\Phi_{T\times T}\psi_{T\times 1})\|^2)^{\dagger\dagger\dagger}$	NTQ_A	$N2T^2Q_A$
	QSM	$\min(\|\phi_{T\times 1}-(\Phi_{T\times T}\psi_{T\times 1})\|^2)^{\dagger\dagger\dagger}$	NT^2Q_A	$N2T^3Q_A$
	SFIM	$\min(\|\phi_{uT\times 1}-(\Phi_{uT\times uT}\psi_{uT\times 1})\|^2)^{\dagger\dagger\dagger\dagger}$	$(N/u)cQ_A^vT$	$(N/u)(cQ_A^vT(uvT+uT))$
	QSFIM	$\min(\|\phi_{uT\times 1}-(\Phi_{uT\times uT}\psi_{uT\times 1})\|^2)^{\dagger\dagger\dagger\dagger}$	$(N/u)cQ_A^vT^2$	$(N/u)(cQ_A^vT^2(uvT+uT))$
	SFDMIM	$\min(\|\phi_{uT\times 1}-(\Phi_{uT\times uT}\psi_{uT\times 1})\|^2)$	$(N/u)cQ_A^vQ_B^{u-v}T$	$(N/u)(cQ_A^vQ_B^{u-v}T(u^2T+uT))$
	QSFDMIM	$\min(\|\phi_{uT\times 1}-(\Phi_{uT\times uT}\psi_{uT\times 1})\|^2)$	$(N/u)cQ_A^vQ_B^{u-v}T^2$	$(N/u)(cQ_A^vQ_B^{u-v}T^2(u^2T+uT))$
SIC	SM	$\phi_{NT\times 1}-\Phi_{NT\times T}\psi_{T\times 1}{}^{\dagger\dagger\dagger}$	N	N^2T
	QSM	$\phi_{NT\times 1}-\Phi_{NT\times T}\psi_{T\times 1}{}^{\dagger\dagger\dagger}$	N	N^2T
	SFIM	$\phi_{NT\times 1}-\Phi_{NT\times uT}\psi_{uT\times 1}{}^{\dagger\dagger\dagger\dagger}$	(N/u)	N^2vT/u
	QSFIM	$\phi_{NT\times 1}-\Phi_{NT\times uT}\psi_{uT\times 1}{}^{\dagger\dagger\dagger\dagger}$	(N/u)	N^2vT/u
	SFDMIM	$\phi_{NT\times 1}-\Phi_{NT\times uT}\psi_{uT\times 1}$	(N/u)	N^2T
	QSFDMIM	$\phi_{NT\times 1}-\Phi_{NT\times uT}\psi_{uT\times 1}$	(N/u)	N^2T

† In every row of $\mathbf{H}_{r,t}$, which is Φ in this case, only N_{Ch} out of N elements are non-zero.
†† The modified Gram-Schmidt orthogonalization algorithm requires $2mn^2$ complex multiplication to compute the QR-factorization of an $m\times n$ matrix.
††† In ψ, only one complex element is nonzero.
†††† In ψ, only v complex elements are nonzero.

matrices, $\phi_{J\times 1}$ and $\psi_{J\times 1}$ are used for $J\times 1$ vectors, $QR(\cdot)$ and $(\cdot)^+$ perform QR decomposition and pseudo-inversion, respectively. The results are summarized in Table 7. According to Table 7, it is observed that whereas the receivers with ML and ZF-SDD detection techniques have the highest and the lowest complexity, respectively, the receivers with ML-SIC and MMSE-JDD techniques provide an intermediate solution in terms of detection complexity.

V. SPECTRAL EFFICIENCY ANALYSIS

As mentioned earlier, GFDM uses a single CP for the entire symbol block composed of K subcarriers with M timeslots. Thus, spectral efficiency gain of GFDM schemes over OFDM schemes with the same system parameters becomes

$$\rho_{GFDM}=100\frac{N_{\mathrm{CP}}(M-1)}{KM+N_{\mathrm{CP}}}\%. \tag{37}$$

As we will show in Section VI, significant gains can be obtained over OFDM schemes in spectral efficiency according to (37). On the other hand, the activation of the QSM operation, i.e., $EN_{QM}=1$, provides a spectral efficiency gain with a negligible increase in detection complexity and slightly decreased BER performance. For instance, spectral efficiency gain of the QSM-GFDM system over SM-OFDM with the same system parameters is given by

$$\rho_{QSM}=100\frac{\log_2(T)}{\log_2(TQ_A)}\%. \tag{38}$$

The spectral efficiency gain provided by the QSM operation is also viable for SFIM and SFDMIM schemes in a decreased manner. Whereas spectral efficiency gain of the QSFIM-GFDM system over SFIM-GFDM with the same system parameters is given by

$$\rho_{QSFIM}=100\frac{\log_2(T)}{\log_2(TcQ_A^v)}\%, \tag{39}$$

TABLE 6. Computational complexity of ML based GFDM-FIM receiver.

Process	*Scheme*	*Operation*	*Execution Count*	*Complexity (CMs)*
Forming $\widetilde{\mathbf{H}}$	all	$\Phi_{N\times N}\Psi_{N\times N}$ ‡	RT	$N_{\mathrm{Ch}}N^2RT$
Block Deinter.	all	No CM	R	0
ML Detection	SM	$\min(\|\phi_{NT\times1}-(\Phi_{NR\times NT}\psi_{NT\times1})\|^2)$ ‡‡	$(Q_AT)^N$	$(Q_AT)^N(N^2R+NT)$
	QSM	$\min(\|\phi_{NT\times1}-(\Phi_{NR\times NT}\psi_{NT\times1})\|^2)$ ‡‡	$(Q_AT^2)^N$	$(Q_AT^2)^N(N^2R+NT)$
	SFIM	$\min(\|\phi_{NT\times1}-(\Phi_{NR\times NT}\psi_{NT\times1})\|^2)$ ‡‡‡	$(cQ_A^vT)^{(N/u)}$	$(cQ_A^vT)^{(N/u)}((N^2Rv/u)+NT)$
	QSFIM	$\min(\|\phi_{NT\times1}-(\Phi_{NR\times NT}\psi_{NT\times1})\|^2)$ ‡‡‡	$(cQ_A^vT^2)^{(N/u)}$	$(cQ_A^vT^2)^{(N/u)}((N^2Rv/u)+NT)$
	SFDMIM	$\min(\|\phi_{NT\times1}-(\Phi_{NR\times NT}\psi_{NT\times1})\|^2)$	$(cQ_A^vQ_B^{u-v}T)^{(N/u)}$	$(cQ_A^vQ_B^{u-v}T)^{(N/u)}(N^2R+NT)$
	QSFDMIM	$\min(\|\phi_{NT\times1}-(\Phi_{NR\times NT}\psi_{NT\times1})\|^2)$	$(cQ_A^vQ_B^{u-v}T^2)^{(N/u)}$	$(cQ_A^vQ_B^{u-v}T^2)^{(N/u)}(N^2R+NT)$

‡ In every row of $\mathbf{H}_{r,t}$, which is Φ in this case, only N_{Ch} out of N elements are non-zero.
‡‡ In ψ, only N complex elements are nonzero.
‡‡‡ In ψ, only Nv/u complex elements are nonzero.

TABLE 7. Summary of the computational complexity of four different receiver structures.

Scheme	*Receiver*	*Complexity (CMs)*
Common Part (CmP)	ZF-SDD	$N^2(2T+R)+N(T^3+2T^2R+TR)$
	MMSE-JDD	$N^3(2T^2R+T^3)+N^2(N_{Ch}RT+RT)$
	ML-SIC	$N^3(2T^2R)+N^2(N_{Ch}RT+RT)$
	ML	$N^2N_{Ch}RT$
SM	ZF-SDD	$\mathrm{CmP}+NT^2Q_A$
	MMSE-JDD	$\mathrm{CmP}+NT^2Q_A$
	ML-SIC	$\mathrm{CmP}+N(2T^2Q_A+NT)$
	ML	$\mathrm{CmP}+(Q_AT)^N(N^2R+NT)$
QSM	ZF-SDD	$\mathrm{CmP}+NT^3Q_A$
	MMSE-JDD	$\mathrm{CmP}+NT^3Q_A$
	ML-SIC	$\mathrm{CmP}+N(2T^3Q_A+NT)$
	ML	$\mathrm{CmP}+(Q_AT^2)^N(N^2R+NT)$
SFIM	ZF-SDD	$\mathrm{CmP}+NcQ_A^vT^2$
	MMSE-JDD	$\mathrm{CmP}+NcQ_A^vT^2$
	ML-SIC	$\mathrm{CmP}+(N/u)(cQ_A^vT(uvT+uT)+vNT)$
	ML	$\mathrm{CmP}+(cQ_A^vT)^{N/u}((N^2Rv/u)+NT)$
QSFIM	ZF-SDD	$\mathrm{CmP}+NcQ_A^vT^3$
	MMSE-JDD	$\mathrm{CmP}+NcQ_A^vT^3$
	ML-SIC	$\mathrm{CmP}+(N/u)((cQ_A^vT^2(uvT+uT)+vNT))$
	ML	$\mathrm{CmP}+(cQ_A^vT^2)^{N/u}((N^2Rv/u)+NT)$
SFDMIM	ZF-SDD	$\mathrm{CmP}+NcQ_A^vQ_B^{u-v}T^2$
	MMSE-JDD	$\mathrm{CmP}+NcQ_A^vQ_B^{u-v}T^2$
	ML-SIC	$\mathrm{CmP}+(N/u)(cQ_A^vQ_B^{u-v}T(u^2T+uT)+uNT)$
	ML	$\mathrm{CmP}+(cQ_A^vQ_B^{u-v}T)^{N/u}(N^2R+NT)$
QSFDMIM	ZF-SDD	$\mathrm{CmP}+NcQ_A^vQ_B^{u-v}T^3$
	MMSE-JDD	$\mathrm{CmP}+NcQ_A^vQ_B^{u-v}T^3$
	ML-SIC	$\mathrm{CmP}+(N/u)(cQ_A^vQ_B^{u-v}T^2(u^2T+uT)+uNT)$
	ML	$\mathrm{CmP}+(cQ_A^vQ_B^{u-v}T^2)^{N/u}(N^2R+NT)$

spectral efficiency gain of the QSFDMIM-GFDM system over SFDMIM-GFDM becomes

$$\rho_{QSFDMIM}=100\frac{\log_2(T)}{\log_2(TcQ_A^vQ_B^{u-v})}\%. \tag{40}$$

Furthermore, enabling DMIM operation, i.e., $EN_{DM}=1$, also provides spectral efficiency gain with a moderately increased detection complexity and slightly decreased BER performance. For instance, spectral efficiency gain of the SFDMIM-GFDM system over SFIM-GFDM with the same system parameters is given by

$$\rho_{SFDMIM}=100\frac{\log_2(Q_B^{u-v})}{\log_2(TcQ_A^v)}\%. \tag{41}$$

Spectral efficiency gains provided by QSM and DMIM operations will be discussed along with the computational complexity and BER performance through numerical results in Section VI.

VI. NUMERICAL ANALYSIS

In this section, uncoded and coded BER performances of the proposed GFDM-FIM schemes are evaluated by computer simulations for Rayleigh fading with Extended Pedestrian A (EPA) channel model [42] using the parameters given in Table 8. The chosen pulse shape for the GFDM prototype filter is the raised cosine (RC) filter.

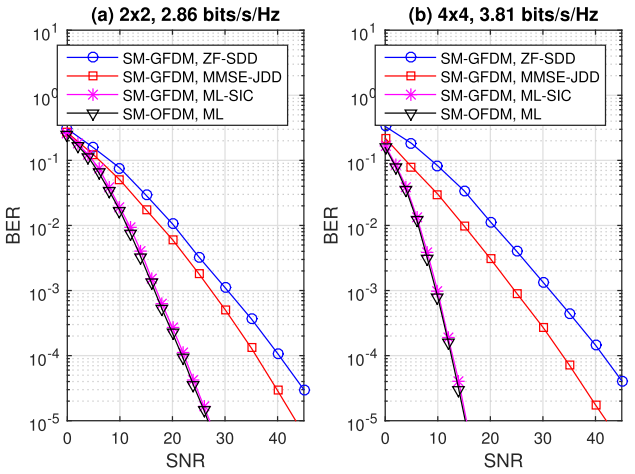

FIGURE 6. Uncoded BER performance of ZF-SDD, MMSE-JDD, ML-SIC and ML detection methods for (a) 2 × 2 (b) 4 × 4 SM schemes using 4-QAM and a roll-off factor of 0.1.

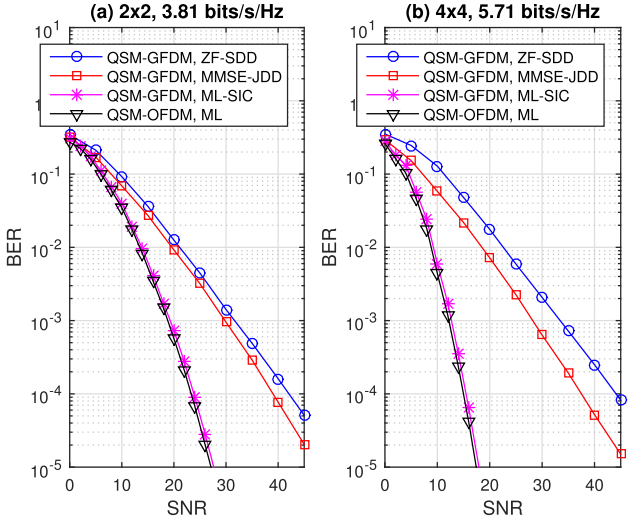

FIGURE 7. Uncoded BER performance of ZF-SDD, MMSE-JDD, ML-SIC and ML detection methods for (a) 2 × 2 (b) 4 × 4 QSM schemes using 4-QAM and a roll-off factor of 0.1.

A. BER PERFORMANCE OF SM AND QSM SCHEMES

Figs. 6 and 7 show the uncoded BER performance of the proposed detection methods for SM-GFDM and QSM-GFDM schemes, respectively, using 4-QAM and a roll-off factor of 0.1. From Fig. 6(a), for a 2 × 2 MIMO configuration and at a BER value of 10^{-4}, it is observed that the proposed ML-SIC scheme achieves 18.1 and 13.7 dB better BER performance than the ZF-SDD and MMSE-JDD detection methods, respectively. In Fig. 6(b), BER performance gains of the ML-SIC scheme with respect to ZF-SDD and MMSE-JDD detection methods for a 4 × 4 MIMO configuration are increased to 28.7 and 21 dB, respectively. Besides, from Figs. 6 and 7, for 2 × 2 and 4 × 4 QSM-GFDM systems using 4-QAM, it is observed that BER performance gains of the ML-SIC scheme with respect to other methods are approximately the same with SM-GFDM counterparts. This significant performance improvement of the ML-SIC detection method arises from the joint detection and demodulation of the transmit antenna indices and the data symbols in a near-optimal manner. In addition, it is observed that increasing the number of antennas enhances the BER performance of the ML-SIC detector. The reason behind this improvement is the increased diversity order of the ML-SIC detector with the number of receive antennas. On the other hand, the number of CMs required to implement the configurations given in Figs. 6 and 7 are given in Tables 9 and 10, respectively. From Tables 9 and 10, as mentioned earlier, it is observed that whereas the receivers with ML and ZF-SDD detection techniques have the highest and the lowest complexity, respectively, the receivers with ML-SIC and MMSE-JDD techniques provide an intermediate solution in terms of detection complexity. Therefore, ML-SIC detection technique can provide an interesting trade-off between complexity and BER performance for SM-GFDM and QSM-GFDM systems.

TABLE 8. Simulation parameters.

Description	*Parameter*	*Value*
Number of subcarriers	K	128
Number of subsymbols	M	5
Pulse shaping filter	g	RC
Length of cyclic prefix	N_{CP}	32
Number of channel taps for EPA channel	N_{Ch}	7

TABLE 9. The total number of CMs for SM-GFDM receivers using 4-QAM.

Ant. Config.	*ZF-SDD*	*MMSE-JDD*	*ML-SIC*	*ML*
2 × 2	2.49×10^{6}	6.31×10^{9}	4.21×10^{9}	1×10^{581}
4 × 4	5.09×10^{6}	5.04×10^{10}	3.36×10^{10}	1×10^{783}

TABLE 10. The total number of CMs for QSM-GFDM receivers using 4-QAM.

Ant. Config.	*ZF-SDD*	*MMSE-JDD*	*ML-SIC*	*ML*
2 × 2	2.50×10^{6}	6.31×10^{9}	4.21×10^{9}	1×10^{783}
4 × 4	5.21×10^{6}	5.04×10^{10}	3.36×10^{10}	1×10^{1157}

Figs. 6 and 7 include BER performances of OFDM applications with ML detection in addition to GFDM schemes. From Figs. 6 and 7, it is observed that BER performances of the SM-GFDM and QSM-GFDM systems with ML-SIC detection are slightly worse than their OFDM counterparts with ML detection. The performance loss of the GFDM schemes with ML-SIC detection is due to nonorthogonal subcarriers and the error propagation of the QR decomposition used in ML-SIC detection. However, according to (37) and Table 8, the GFDM schemes provide 19% spectral efficiency gain over the OFDM schemes. Furthermore, from (38) and Table 8, it is observed that spectral efficiency gains of QSM-GFDM scheme over SM-GFDM schemes using 4-QAM become 33% and 50% for 2 × 2 and 4 × 4 MIMO configurations, respectively, with a negligible increase in detection complexity and slightly decreased BER performance.

Fig. 8(a) compares the uncoded BER performances of the 2 × 2 SM-GFDM system using 8-QAM and the 2 × 2

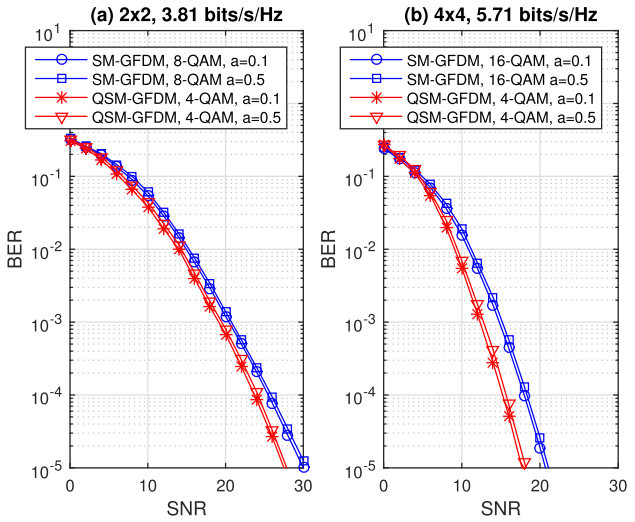

FIGURE 8. Uncoded BER performance of SM-GFDM and QSM-GFDM schemes using ML-SIC detection method for (a) 2 × 2 (b) 4 × 4 with 4-QAM and roll-off factors (a) of 0.1 and 0.5.

QSM-GFDM system using 4-QAM with the ML-SIC detection method considering roll-off factors of 0.1 and 0.5 in order to achieve the same spectral efficiency. The results in Fig. 8(a) demonstrate that the QSM-GFDM scheme provides approximately 1.8 dB BER gain with respect to SM-GFDM scheme for the 2×2 MIMO configuration at a BER value of 10^{-4}. Besides, from Fig. 8(b), it is observed that 4×4 QSM-GFDM system using 4-QAM provides approximately 2.8 dB BER gain with respect to 4×4 SM-GFDM system using 16-QAM. On the other hand, according to Tables 7 and 8, the computational complexity of the ML-SIC based 2×2 SM-GFDM receiver for 8-QAM and 4×4 SM-GFDM receiver for 16-QAM are on the order of 4.21×10^9 and 3.36×10^{10}, respectively. By comparing these results with the computational complexity of 2×2 QSM-GFDM receiver for 4-QAM and 4×4 QSM-GFDM receiver for 4-QAM in Table 10, it is observed that these improvements are provided at no additional complexity. Furthermore, from Figs. 8(a) and 8(b), it is observed that increasing the roll-off factor slightly degrades the performance.

B. BER PERFORMANCE OF SFIM AND QSFIM SCHEMES

Figs. 9 and 10 show the uncoded BER performance of the proposed detection methods for SFIM and QSFIM schemes, respectively, using 4-QAM and a roll-off factor of 0.1. Here, the look-up table given in Table 11 is used to determine the IM subgroups. From Fig. 9(a), for a 2×2 MIMO configuration and at a BER value of 10^{-4}, it is observed that the proposed ML-SIC scheme achieves 25.7 and 13.4 dB better BER performance than the ZF-SDD and MMSE-JDD detection methods, respectively. In Fig. 9(b), for a 4×4 MIMO configuration, BER performance gains of the ML-SIC scheme with respect to ZF-SDD and MMSE-JDD detection methods are increased to 32.8 and 15.8 dB, respectively. From Figs. 9 and 10, for QSFIM scheme, it is observed that

TABLE 11. A look-up table example for IM subgroups with $u = 4$ and $v = 2$.

Bits	*Indices*	*subblocks*
[0 0]	{1, 2}	$[s_\chi \quad s_\zeta \quad 0 \quad 0]^T$
[0 1]	{2, 3}	$[0 \quad s_\chi \quad s_\zeta \quad 0]^T$
[1 0]	{3, 4}	$[0 \quad 0 \quad s_\chi \quad s_\zeta]^T$
[1 1]	{1, 4}	$[s_\chi \quad 0 \quad 0 \quad s_\zeta]^T$

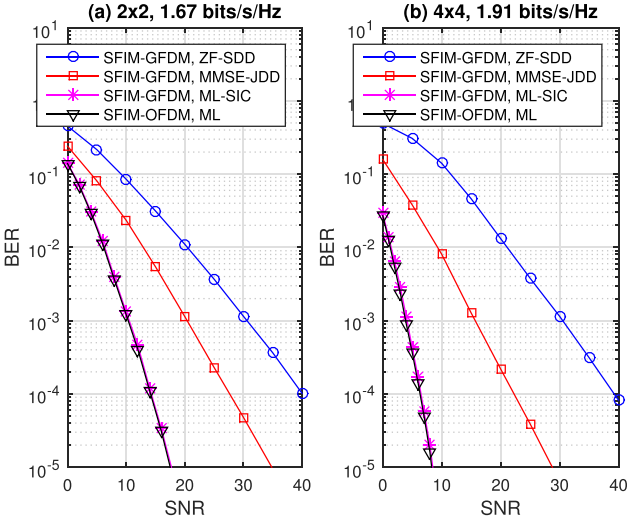

FIGURE 9. Uncoded BER performance of ZF-SDD, MMSE-JDD, ML-SIC and ML detection methods for (a) 2 × 2 (b) 4 × 4 SFIM schemes using 4-QAM and a roll-off factor of 0.1.

BER performance gains of the ML-SIC scheme with respect to other methods are approximately the same with the gains in SFIM systems as in the cases of SM and QSM. The significant performance improvements observed in Figs. 9 and 10 are due to joint detection and demodulation of the transmit antenna indices and the active subcarrier indices as well as QAM data symbols and the increased diversity order of ML-SIC. On the other hand, the number of CMs required to implement the configurations given in Figs. 9 and 10 are given in Tables 12 and 13, respectively. From Tables 12 and 13, it is observed that an interesting trade-off between complexity and BER performance is also valid for SFIM-GFDM and QSFIM-GFDM systems when ML-SIC detection is used. Besides, according to (39) and Table 8, QSFIM-GFDM schemes provide 14% and 25% spectral efficiency gains over SFIM-GFDM schemes for 2×2 and 4×4 MIMO configurations, respectively, with a negligible increase in detection complexity and slightly decreased BER performance. Additionally, the performance loss of the GFDM systems using ML-SIC detection with respect to OFDM systems is also observed for SFIM and QSFIM schemes.

Fig. 11(a) investigates the effects of combination of SM and IM schemes in terms of uncoded BER performance and spectral efficiency for ML-SIC detection method using a roll-off factor of 0.1. From Fig. 11(a), at a BER value of 10^{-4}, it is observed that 4×4 SFIM-GFDM system for binary

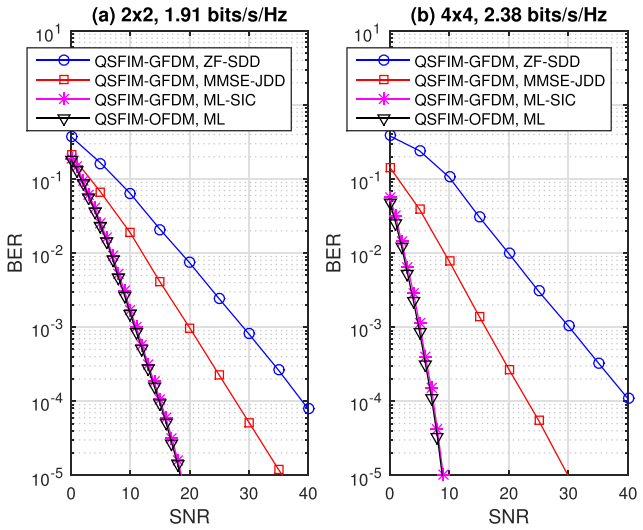

FIGURE 10. Uncoded BER performance of ZF-SDD, MMSE-JDD, ML-SIC and ML detection methods for (a) 2 × 2 (b) 4 × 4 QSFIM schemes using 4-QAM and a roll-off factor of 0.1.

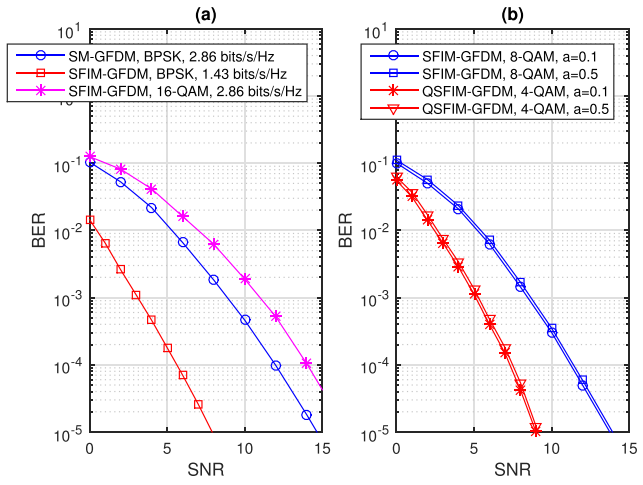

FIGURE 11. Uncoded BER performance comparisons of SFIM-GFDM with (a) SM-GFDM with a roll-off factor of 0.1 (b) QSFIM-GFDM with roll-off factors (a) of 0.1 and 0.5, for a 4 × 4 MIMO configuration with ML-SIC detection method.

TABLE 12. The total number of CMs for SFIM-GFDM receivers using 4-QAM.

Ant. Config.	*ZF-SDD*	*MMSE-JDD*	*ML-SIC*	*ML*
2 × 2	2.64×10^6	6.30×10^9	4.21×10^9	1×10^{341}
4 × 4	5.70×10^6	5.04×10^{10}	3.36×10^{10}	1×10^{389}

TABLE 13. The total number of CMs for QSFIM-GFDM receivers using 4-QAM.

Ant. Config.	*ZF-SDD*	*MMSE-JDD*	*ML-SIC*	*ML*
2 × 2	2.80×10^6	6.31×10^9	4.21×10^9	1×10^{389}
4 × 4	7.67×10^6	5.04×10^{10}	3.36×10^{10}	1×10^{485}

PSK (BPSK) provides approximately 6.4 dB BER gain with respect to 4 × 4 SM-GFDM system for BPSK at the same computational complexity. Note that, for this configuration, spectral efficiency of the SFIM-GFDM scheme is the half as that of the SM-GFDM scheme. On the other hand, 4 × 4 SM-GFDM system for BPSK achieves 2 dB better BER performance than 4 × 4 SFIM-GFDM system for 16-QAM at the same spectral efficiency. The BER performance gain of the SFIM scheme is due to the improved Euclidean distance spectrum of IM. As a result, it is observed that SFIM scheme can provide an interesting trade-off between spectral efficiency and BER performance.

Fig. 11(b) shows the uncoded BER performances of the 4 × 4 SFIM-GFDM system for 8-QAM and the 4 × 4 QSFIM-GFDM system for 4-QAM considering a roll-off factor of 0.1 and 0.5 in order to achieve the same spectral efficiency. The results in Fig. 11 demonstrate that the QSFIM-GFDM scheme provides approximately 3.9 dB BER gain with respect to SFIM-GFDM scheme for the 4 × 4 MIMO configuration and at a BER value of 10^{-4}. On the other hand, according to Tables 7 and 8, the computational complexity of the ML-SIC based 4 × 4 SFIM-GFDM receiver for 8-QAM is on the order of 3.36×10^{10}. By comparing this result with the computational complexity of 4 × 4 QSFIM-GFDM receiver for 4-QAM in Table 13, it is observed that this improvement is provided at no additional complexity. Besides, the results show that slight degradation of BER performance due to increased roll-off factor is also valid for SFIM-GFDM and QSFIM-GFDM schemes.

Fig. 12 compares the uncoded BER performances of SM, IM and QAM parts of the SFIM scheme for a 4 × 4 MIMO configuration with ML-SIC detection method using 4-QAM and a roll-off factor of 0.1. From Fig. 12, it is observed that SM part has 2 dB better BER performance with respect to overall SFIM BER. As a result, by proper mapping at the primary and the secondary bit splitter parts of the transmitter, information bits, which need high reliability, can be transmitted through antenna indices and thus, SFIM scheme provides an extra level of flexibility.

C. BER PERFORMANCE OF SFDMIM AND QSFDMIM SCHEMES

Figs. 13 and 14 show the uncoded BER performance of the proposed detection methods for SFDMIM and QSFDMIM schemes, respectively, using 4-QAM and a roll-off factor of 0.1. In order to determine the primary and secondary IM subgroups, the look-up table given in Table 14 is used. For DMIM operation, an 8-level QAM constellation, illustrated in Fig. 15 is employed. The DMIM constellations are defined as $\mathcal{S}^A = \left\{(1+j)/\sqrt{6}, (-1+j)/\sqrt{6}, (1-j)/\sqrt{6}, (-1-j)/\sqrt{6}\right\}$ and $\mathcal{S}^B = \left\{(3+j)/\sqrt{6}, (-3+j)/\sqrt{6}, (3-j)/\sqrt{6}, (-3-j)/\sqrt{6}\right\}$ for Mapper A and Mapper B, respectively. From Fig. 13(a), for a 2 × 2 MIMO configuration and at a BER value of 10^{-4}, it is observed that the proposed ML-SIC scheme achieves 21.2 and 15.9 dB better BER performance than the ZF-SDD and MMSE-JDD detection methods, respectively.

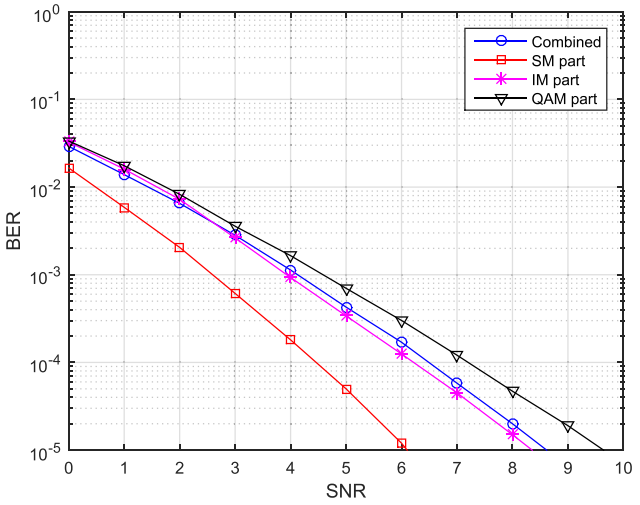

FIGURE 12. Uncoded BER performance comparisons of SM, IM and QAM parts of SFIM-GFDM scheme for a 4 × 4 MIMO configuration with ML-SIC detection method using 4-QAM and a roll-off factor of 0.1.

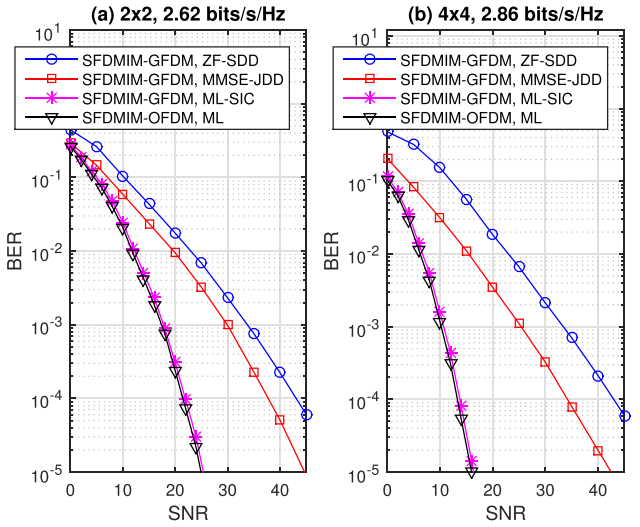

FIGURE 13. Uncoded BER performance of ZF-SDD, MMSE-JDD, ML-SIC and ML detection methods for (a) 2 × 2 (b) 4 × 4 SFDMIM schemes using 4-QAM and a roll-off factor of 0.1.

TABLE 14. A look-up table example for DMIM subgroups with $u = 4, v = 2$.

Bits	*Indices*	*subgroups*
[0 0]	{1, 2}	$[s_l^A(1) \;\; s_l^A(2) \;\; s_l^B(1) \;\; s_l^B(2)]^T$
[0 1]	{2, 3}	$[s_l^B(1) \;\; s_l^A(1) \;\; s_l^A(2) \;\; s_l^B(2)]^T$
[1 0]	{3, 4}	$[s_l^B(1) \;\; s_l^B(2) \;\; s_l^A(1) \;\; s_l^A(2)]^T$
[1 1]	{1, 4}	$[s_l^A(1) \;\; s_l^B(1) \;\; s_l^B(2) \;\; s_l^A(2)]^T$

In Fig. 13(b), for 4 × 4 MIMO configuration, BER performance gains of the ML-SIC scheme with respect to ZF-SDD and MMSE-JDD detection methods were increased to 29.2 and 20.4 dB, respectively. From Fig. 14, for QSFDMIM scheme, it is observed that BER performance gains of the ML-SIC scheme are approximately the same with

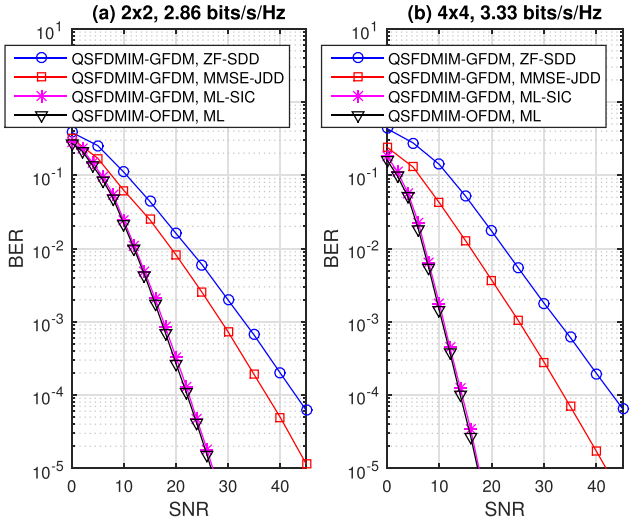

FIGURE 14. Uncoded BER performance of ZF-SDD, MMSE-JDD, ML-SIC and ML detection methods for (a) 2 × 2 (b) 4 × 4 QSFDMIM schemes using 4-QAM and a roll-off factor of 0.1.

TABLE 15. The total number of CMs for SFDMIM-GFDM receivers using 4-QAM.

Ant. Config.	*ZF-SDD*	*MMSE-JDD*	*ML-SIC*	*ML*
2 × 2	5.10×10^6	6.31×10^9	4.22×10^9	1×10^{533}
4 × 4	1.55×10^7	5.04×10^{10}	3.37×10^{10}	1×10^{581}

TABLE 16. The total number of CMs for QSFDMIM-GFDM receivers using 4-QAM.

Ant. Config.	*ZF-SDD*	*MMSE-JDD*	*ML-SIC*	*ML*
2 × 2	7.72×10^6	6.31×10^9	4.23×10^9	1×10^{581}
4 × 4	4.70×10^7	5.04×10^{10}	3.38×10^{10}	1×10^{677}

the SFDMIM system. On the other hand, the number of CMs required to implement the configurations given in Figs. 13 and 14 are given in Tables 15 and 16, respectively. From Tables 15 and 16, it is observed that the interesting trade-off between complexity and BER performance is also valid for SFDMIM-GFDM and QSFDMIM-GFDM systems when ML-SIC detection is used. Furthermore, from (41) and Table 8, it is observed that spectral efficiency gains of SFDMIM-GFDM scheme over SFIM-GFDM schemes using 4-QAM become 57% and 50% for 2 × 2 and 4 × 4 MIMO configurations, respectively. On the other hand, from (40) and Table 8, it is observed that spectral efficiency gains of QSFDMIM-GFDM scheme over SFDMIM-GFDM schemes using 4-QAM become 9% and 16% for 2 × 2 and 4 × 4 MIMO configurations, respectively. For both cases, a negligible increase in detection complexity and a slightly decreased BER performance are noticed. Additionally, the performance loss of the GFDM systems using ML-SIC detection with respect to OFDM systems is also observed for SFDMIM and QSFDMIM schemes.

Fig. 16 investigates the effect of DMIM operation in terms of uncoded BER performances for a 4 × 4 MIMO configuration with ML-SIC detection method and a roll-off factor

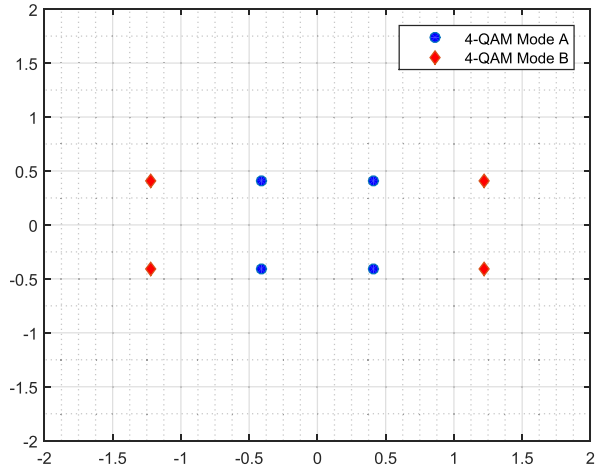

FIGURE 15. An example of DMIM constellation design for Q_A and Q_B with $Q_A = Q_B = 4$.

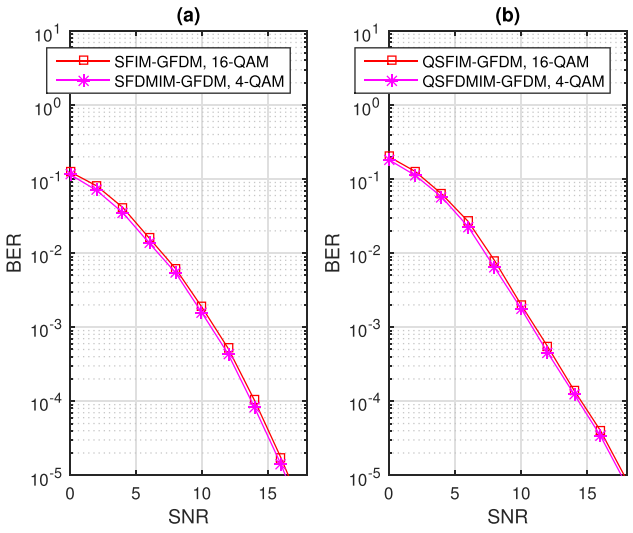

FIGURE 16. Uncoded BER performance comparisons of IM and DMIM schemes using ML-SIC detection method for a 4 × 4 MIMO configuration and a roll-off factor of 0.1. (a) SFIM vs SFDMIM (b) QSFIM vs QSFDMIM.

of 0.1. From Fig. 16, at a BER value of 10^{-4}, it is observed that using DMIM scheme instead of IM provides 0.2 dB BER gain for both SFIM and QSFIM schemes at the same spectral efficiency. On the other hand, according to Tables 7 and 8, the computational complexity of the ML-SIC based 4 × 4 SFIM-GFDM receiver for 16-QAM and 4×4 QSFIM-GFDM receiver for 16-QAM are on the order of 3.36×10^{10} and 3.37×10^{10}, respectively. By comparing these results with the computational complexity of 4×4 SFDMIM-GFDM receiver for 4-QAM and 4×4 QSFDMIM-GFDM receiver for 4-QAM in Tables 15 and 16, respectively, it is observed that these improvements are provided with increased computational complexity.

D. CODED BER PERFORMANCE ANALYSIS

Fig. 17 shows the coded BER performances of the GFDM-FIM schemes for a 4 × 4 MIMO configuration with ML-SIC detection method using 4-QAM and a roll-off factor of 0.1.

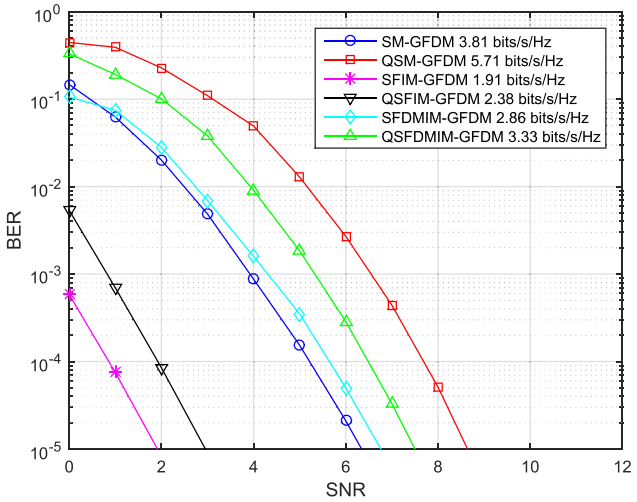

FIGURE 17. Coded BER performance of the convolutional coded GFDM-FIM schemes using ML-SIC detection method for a 4 × 4 MIMO configuration with 4-QAM and a roll-off factor of 0.1.

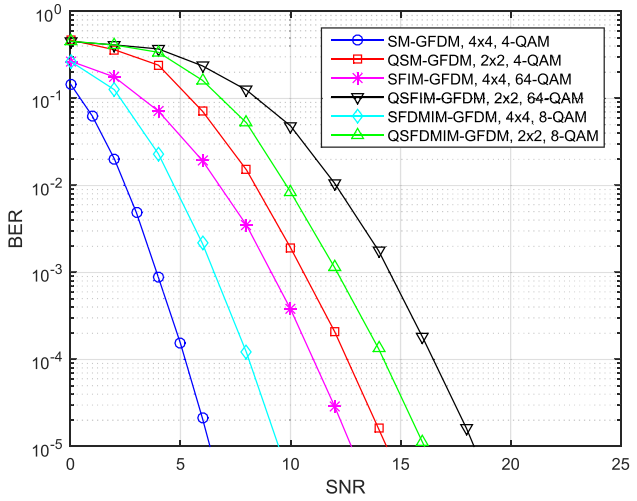

FIGURE 18. Coded BER performance of the convolutional coded GFDM-FIM schemes using ML-SIC detection method and a roll-off factor of 0.1 for 3.81 bits/s/Hz spectral efficiency.

For the channel code, the rate 1/3 convolutional code with generator sequence $q = [133, 171, 165]$ was chosen [43]. From Fig. 17, it is observed that channel coding provides significant BER gains between 5.4 and 8.1 dB with respect to uncoded schemes. Note that coded BER performances get worse with the increasing spectral efficiency.

Fig. 18 compares the coded BER performances of the GFDM-FIM schemes using ML-SIC detection method and a roll-off factor of 0.1 for 3.81 bits/s/Hz spectral efficiency. Here, a 16-level QAM constellation, illustrated in Fig. 19 is employed for 8-QAM DMIM operation. The DMIM constellations are defined as $\mathcal{S}^A = \{(-3+j)/\sqrt{10}, (-3-j)/\sqrt{10}, (-1+j)/\sqrt{10}, (-1-j)/\sqrt{10}, (3+j)/\sqrt{10}, (3-j)/\sqrt{10}, (1+j)/\sqrt{10}, (1-j)/\sqrt{10}\}$ and $\mathcal{S}^B = \{(-3+3j)/\sqrt{10}, (-3-3j)/\sqrt{10}, (-1+3j)/\sqrt{10}, (-1-3j)/\sqrt{10}, (3+3j)/\sqrt{10}, (3-3j)/\sqrt{10}, (1+3j)/\sqrt{10}, (1-3j)/\sqrt{10}\}$ for Mapper

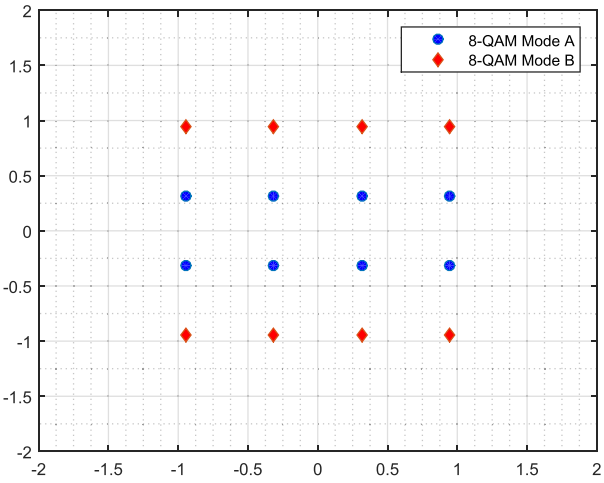

FIGURE 19. An example of DMIM constellation design for Q_A and Q_B with $Q_A = Q_B = 8$.

TABLE 17. Computational complexities sorted from the lowest to the highest for a 4 × 4 MIMO configuration with 4-QAM.

Order	*Scheme & Detection Method*
1	SM, ZF-SDD
2	QSM, ZF-SDD
3	SFIM, ZF-SDD
4	QSFIM, ZF-SDD
5	SFDMIM, ZF-SDD
6	QSFDMIM, ZF-SDD
7	SM, ML-SIC
8	QSM, ML-SIC
9	SFIM, ML-SIC
10	QSFIM, ML-SIC
11	SFDMIM, ML-SIC
12	QSFDMIM, ML-SIC
13	SM, MMSE-JDD
14	QSM, MMSE-JDD
15	SFIM, MMSE-JDD
16	QSFIM, MMSE-JDD
17	SFDMIM, MMSE-JDD
18	QSFDMIM, MMSE-JDD

A and Mapper B, respectively. From Fig. 18, it is observed that the BER performances of the GFDM-FIM schemes for a 4 × 4 MIMO configuration are significantly better than that of the GFDM-FIM schemes for a 2 × 2 MIMO configuration independent of the modulation order. Therefore, it can be stated that the coded BER performances of the GFDM-FIM schemes using ML-SIC detection method are mainly determined by the number of receive antennas. Besides, it is observed that the coded BER performances of the GFDM-FIM schemes become worse with the increasing modulation order for the same number of receive antennas. Thus, it can be stated that the modulation order is a secondary factor on the coded BER performances of the GFDM-FIM schemes using the ML-SIC detection method.

VII. DISCUSSION

In this section, the obtained numerical results for BER performance, computational complexity and spectral efficiency are discussed. Then, based on these results, a recommendation table for selecting the proper GFDM-FIM scheme considering performance criterion is given. The obtained numerical results are summarized below:

1. SM, IM, and SFIM schemes along with the QSM and DMIM variants are all applicable with GFDM.

2. Suboptimal ZF-SDD and MMSE-JDD detection methods and near optimal ML-SIC detection method can be used with all proposed MIMO-GFDM applications.

3. ML-SIC detection method provides significant BER performance gains with respect to ZF-SDD and MMSE-JDD detection methods at the cost of increased computational complexity. This significant performance improvements arise from the joint detection and demodulation of spatial and frequency indices as well as QAM data symbols in a near-optimal manner. Therefore, ML-SIC detection technique can provide an interesting trade-off between complexity and BER performance.

4. BER performance of the ML-SIC detection method increases with increasing number of receive antennas. The reason behind this improvement is the increased diversity order of the ML-SIC detector with the number of receive antennas.

5. BER performance of the ML-SIC detection methods are slightly worse than their OFDM counterparts with ML detection. This performance loss is due to nonorthogonal subcarriers and the error propagation of the QR decomposition.

TABLE 18. Required Transmit Power sorted from the lowest to the highest to achieve a BER value of 10^{-4} for a 4 × 4 MIMO configuration with 4-QAM.

Order	*Scheme & Detection Method*
1	SFIM, ML-SIC
2	QSFIM, ML-SIC
3	SM, ML-SIC
4	SFDMIM, ML-SIC
5	QSFDMIM, ML-SIC
6	QSM, ML-SIC
7	SFIM, MMSE-JDD
8	QSFIM, MMSE-JDD
9	SM, MMSE-JDD
10	SFDMIM, MMSE-JDD
11	QSFDMIM, MMSE-JDD
12	QSM, MMSE-JDD
13	SFIM, ZF-SDD
14	QSFIM, ZF-SDD
15	SM, ZF-SDD
16	SFDMIM, ZF-SDD
17	QSFDMIM, ZF-SDD
18	QSM, ZF-SDD

TABLE 19. Spectral Efficiencies sorted from the highest to the lowest for a 4 × 4 MIMO configuration with 4-QAM.

Order	*Scheme*
1	QSM
2	SM
3	QSFDMIM
4	SFDMIM
5	QSFIM
6	SFIM

TABLE 20. Recommendations about selecting the proper GFDM-FIM scheme.

Complexity	*Transmit Power*	*Spectral Efficiency*	*Scheme*	*Receiver*
Lowest	Low	Do not care	SM	ZF-SDD
Lowest	Do not care	High	QSM	ZF-SDD
Low	Lowest	Do not care	SFIM	ML-SIC
Do not care	Lowest	High	QSFIM	ML-SIC
Low	Do not care	Highest	SM	ZF-SDD
Do not care	Low	Highest	QSM	ZF-SDD
Moderate	Moderate	Do not care	SFDMIM	ML-SIC
Moderate	Do not care	Moderate	QSFDMIM	ML-SIC
Do not care	Moderate	Moderate	SFDMIM	MMSE-JDD

Note that for this case, GFDM provides significant spectral efficiency gains with respect to OFDM.

6. Enabling QSM operation provides significant spectral efficiency gains with a negligible increase in detection complexity and slightly decreased BER performance. On the other hand, QSM operation provides BER performance gains at the same spectral efficiency with no additional complexity.

7. Increasing the roll-off factor of the pulse shaping filter slightly degrades the performance of the GFDM-FIM schemes.

8. SFIM schemes provides BER performance gain at the cost of decreased spectral efficiency. This BER performance gain is due to the improved Euclidean distance spectrum of IM. Therefore SFIM scheme can provide an interesting trade-off between spectral efficiency and BER performance.

9. Enabling DMIM operation provides significant spectral efficiency gains with an increased detection complexity and slightly decreased BER performance. On the other hand, DMIM operation improves the BER performance slightly at the same spectral efficiency with additional complexity.

10. Thanks to using space and frequency indices together, proposed SFIM scheme provides a multilayer scheme, which reveals different BER performances and spectral efficiencies. In this context, information bits transmitted through antenna indices has an extra 2 dB BER performance gain in addition to SFIM BER gain. As a result, SFIM scheme has a strong potential to support different use-cases by using common space, frequency and time resources at the same time.

11. Channel coding improves the BER performance of the GFDM-FIM scheme as expected.

12. The coded BER performances of the GFDM-FIM schemes using ML-SIC detection method are mainly determined by the number of receive antennas. Besides, the modulation order is the secondary factor on the coded BER performances of the GFDM-FIM schemes using ML-SIC detection method.

In Table 17, the proposed MIMO-GFDM applications are sorted from the lowest to the highest in terms of the computational complexity for a 4×4 MIMO configuration with 4-QAM transmission. As stated earlier, ZF-SDD detection method has the lowest complexity among the proposed detection methods, since QSM, IM, and DMIM operations increase the computational complexity. Table 18 lists the proposed MIMO-GFDM applications from the lowest transmit power to the highest transmit power for a 4×4 MIMO configuration with 4-QAM transmission at a BER value of 10^{-4}. It is observed that, SFIM scheme needs the lowest transmit power to reach the desired BER value. In Table 19, the proposed MIMO-GFDM applications are ranked from the highest to the lowest in terms of spectral efficiency for a 4×4 MIMO configuration with 4-QAM transmission. According to these results, QSM-GFDM has the highest spectral efficiency among the proposed schemes. According to Tables 17, 18 and 19, it is obvious that there is not any scheme, which has best performance for all performance criterion at the same time. Therefore, performance criterion have to be prioritized and the proper scheme must be selected considering the related criterion among the proposed MIMO-GFDM schemes. In Table 20, based on the results in Tables 17, 18 and 19, a recommendation table to select the proper MIMO-GFDM scheme is given considering various emphasis of complexity, spectral efficiency and transmit power criterion. Table 20 shows that GFDM-FIM has a strong potential to engineer the space-frequency structure according to channel conditions and use-cases and provides a great flexibility, which can be easily tuned to address the required performance criterion.

VIII. CONCLUSION

As the massive growth trend in number of wireless devices and applications continues, novel RATs including advanced waveforms and more flexible radio accessing schemes will be a necessity. In this paper, based on the advantages of non-CP-OFDM-based waveforms and the IM concept, an FIM framework, which combines GFDM with space and frequency IM schemes, has been proposed and novel transmitter and receiver schemes for MIMO-GFDM applications have been presented.

The proposed framework has an FIM transmitter, which is capable of generating six different SFIM schemes. For the receiver part, a near-optimum detection scheme, which is based on ML detection with SIC, has been proposed. The FIM receiver provides different levels of BER performances and computational complexities by the proposed ML-SIC detection scheme and the ZF-SDD and MMSE-JDD detection schemes existing in the literature. Thanks to the proposed FIM transmitter and receiver structures, transmission scheme and the detection method can be determined

according to desired level of complexity, transmit power and spectral efficiency of the use-cases. Besides, switching between different IM schemes according to channel conditions can be possible using a single transceiver structure. Furthermore, FIM framework provides a multilayer scheme by means of different levels of BER performances and spectral efficiencies and enables to support different use-cases by using common space, frequency, and time resources at the same time. It has been shown that GFDM-FIM has a strong potential to engineer the space-frequency structure according to channel conditions and use-cases as well as it provides a great flexibility, which can be easily tuned to address the required performance criterion.

As mentioned earlier, GFDM has a flexibility to engineer the time-frequency structure and beneficial properties to fulfill the requirements of future wireless networks. By integrating GFDM with promising space and frequency indexing schemes in a skilled framework, GFDM-FIM can be considered a promising PHY layer technique for future wireless networks. Our future work will focus on theoretical analysis which can provide more insights on the impact of some parameters on the system performance for systematic optimization.

REFERENCES

[1] G. Wunder *et al.*, "5GNOW: Non-orthogonal, asynchronous waveforms for future mobile applications," *IEEE Commun. Mag.*, vol. 52, no. 2, pp. 97–105, Feb. 2014.

[2] *IMT Vision Framework and Overall Objectives of the Future Development of IMT for 2020 and Beyond*, document M.2083-0, ITU-R, Sep. 2015.

[3] *Study on Scenarios and Requirements for Next Generation Access Technologies*, document 38.913, 3GPP, Feb. 2016.

[4] J. Abdoli *et al.*, "Filtered OFDM: A new waveform for future wireless systems," in *Proc. IEEE Int. Workshop Signal Process. Adv. Wireless Commun.*, Stockholm, Sweden, Jun. 2015, pp. 66–70.

[5] X. Zhang, M. Jia, L. Chen, J. Ma, and J. Qiu, "Filtered-OFDM—Enabler for flexible waveform in the 5th generation cellular networks," in *Proc. IEEE GLOBECOM Workshops*, San Diego CA, USA, Dec. 2015, pp. 1–6.

[6] E. Bala, J. Li, and R. Yang, "Shaping spectral leakage: A novel low-complexity transceiver architecture for cognitive radio," *IEEE Veh. Technol. Mag.*, vol. 8, no. 3, pp. 38–46, Sep. 2013.

[7] N. Michailow *et al.*, "Generalized frequency division multiplexing for 5th generation cellular networks," *IEEE Trans. Commun.*, vol. 62, no. 9, pp. 3045–3061, Sep. 2014.

[8] M. Matthe, L. L. Mendes, and G. Fettweis, "Space-time coding for generalized frequency division multiplexing," in *Proc. 20th Eur. Wireless Conf.*, Barcelona, Spain, May 2014, pp. 1–5.

[9] M. Matthe, L. L. Mendes, I. Gaspar, N. Michailov, D. Zhang, and G. Fettweis, "Widely linear estimation for space-time-coded GFDM in low latency applications," *IEEE Trans. Commun.*, vol. 63, no. 11, pp. 4501–4509, Nov. 2015.

[10] M. Matthe, L. L. Mendes, I. Gaspar, N. Michailov, D. Zhang, and G. Fettweis, "Multi-user time-reversal STC-GFDMA for future wireless networks," *EURASIP J. Wireless Commun. Netw.*, vol. 2015, no. 1, pp. 1–8, May 2015.

[11] D. Zhang, L. L. Mendes, M. Matthe, N. Michailov, and G. Fettweis, "Expectation propagation for near-optimum detection of MIMO-GFDM signals," *IEEE Trans. Wireless Commun.*, vol. 15, no. 2, pp. 1045–1062, Feb. 2016.

[12] D. Zhang, L. L. Mendes, M. Matthe, and G. Fettweis, "A Markov chain Monte Carlo algorithm for near-optimum detection of MIMO-GFDM signals," in *Proc. IEEE Pers., Indoor Mobile Radio Commun. (PIMRC)*, Aug. 2015, pp. 1–5.

[13] N. Tunali, M. Wu, C. Dick, C. Studer, and S. Jose, "Linear large-scale MIMO data detection for 5G multi-carrier waveform candidates," in *Proc. Asilomar Conf. Signals, Syst., Comput.*, Nov. 2015, pp. 1–5.

[14] M. Matthe, I. Gaspar, D. Zhang, and G. Fettweis, "Near-ML detection for MIMO-GFDM," in *Proc. 82nd IEEE Veh. Technol. Conf. Fall*, Boston, MA, USA, Sep. 2015, pp. 1–2.

[15] M. Matthe, D. Zhang, and G. Fettweis, "Iterative detection using MMSE-PIC demapping for MIMO-GFDM systems," in *Proc. IEEE Eur. Wireless (EW)*, May 2016, pp. 1–7.

[16] M. Matthe, D. Zhang, and G. Fettweis, "Sphere-decoding aided SIC for MIMO-GFDM: Coded performance analysis," in *Proc. Int. Symp. Wireless Commun. Syst. (ISWCS)*, Poznan, Poland, Sep. 2016, pp. 165–169.

[17] D. Zhang, M. Matthe, L. L. Mendes, and G. Fettweis, "A study on the link level performance of advanced multicarrier waveforms under MIMO wireless communication channels," *IEEE Trans. Wireless Commun.*, vol. 16, no. 4, pp. 2350–2365, Apr. 2017.

[18] R. Y. Mesleh, H. Haas, S. Sinanovic, C. W. Ahn, and S. Yun, "Spatial modulation," *IEEE Trans. Veh. Technol.*, vol. 57, no. 4, pp. 2228–2241, Jul. 2008.

[19] R. Mesleh, S. Ikki, and H. Aggoune, "Quadrature spatial modulation," *IEEE Trans. Veh. Technol.*, vol. 64, no. 6, pp. 2738–2742, Jun. 2015.

[20] E. Basar, Ü. Aygölü, E. Panayırcı, and H. V. Poor, "Orthogonal frequency division multiplexing with index modulation," *IEEE Trans. Signal Process.*, vol. 61, no. 22, pp. 5536–5549, Nov. 2013.

[21] R. Abu-alhiga and H. Haas, "Subcarrier-index modulation OFDM," in *Proc. IEEE Int. Symp. Pers., Indoor Mobile Radio Commun.*, Tokyo, Japan, Sep. 2009, pp. 177–181.

[22] D. Tsonev, S. Sinanovic, and H. Haas, "Enhanced subcarrier index modulation (SIM) OFDM," in *Proc. IEEE GLOBECOM Workshops*, Dec. 2011, pp. 728–732.

[23] T. Mao, Z. Wang, Q. Wang, S. Chen, and L. Hanzo, "Dual-mode index modulation aided OFDM," *IEEE Access*, vol. 5, pp. 50–60, 2016.

[24] M. Wen, E. Basar, Q. Li, B. Zheng, and M. Zhang, "Multiple-mode orthogonal frequency division multiplexing with index modulation," *IEEE Trans. Commun.*, vol. 65, no. 9, pp. 3892–3906, Sep. 2017.

[25] E. Basar, "OFDM with index modulation using coordinate interleaving," *IEEE Wireless Commun. Lett.*, vol. 4, no. 4, pp. 381–384, Aug. 2015.

[26] R. Fan, Y. J. Yu, and Y. L. Guan, "Generalization of orthogonal frequency division multiplexing with index modulation," *IEEE Trans. Wireless Commun.*, vol. 14, no. 10, pp. 5350–5359, Oct. 2015.

[27] M. Wen, Y. Zhang, J. Li, E. Basar, and F. Chen, "Equiprobable subcarrier activation method for OFDM with index modulation," *IEEE Commun. Lett.*, vol. 20, no. 12, pp. 2386–2389, Dec. 2016.

[28] M. Wen, B. Ye, E. Basar, Q. Li, and F. Ji, "Enhanced orthogonal frequency division multiplexing with index modulation," *IEEE Trans. Wireless Commun.*, vol. 16, no. 7, pp. 4786–4801, Jul. 2017.

[29] H. Zhang, L. L. Yang, and L. Hanzo, "Compressed sensing improves the performance of subcarrier index-modulation-assisted OFDM," *IEEE Access*, vol. 4, pp. 7859–7873, Oct. 2016.

[30] E. Başar, "Multiple-input multiple-output OFDM with index modulation," *IEEE Signal Process. Lett.*, vol. 22, no. 12, pp. 2259–2263, Sep. 2015.

[31] T. Datta, H. S. Eshwaraiah, and A. Chockalingam, "Generalized space-and-frequency index modulation," *IEEE Trans. Veh. Technol.*, vol. 65, no. 7, pp. 4911–4924, Jul. 2016.

[32] E. Basar, "On multiple-input multiple-output OFDM with index modulation for next generation wireless networks," *IEEE Trans. Signal Process.*, vol. 64, no. 15, pp. 3868–3878, Aug. 2016.

[33] B. Zheng, M. Wen, E. Basar, and F. Chen, "Multiple-input multiple-output OFDM with index modulation: Low-complexity detector design," *IEEE Trans. Signal Process.*, vol. 65, no. 11, pp. 2758–2772, Jun. 2017.

[34] E. Basar *et al.*, "Index modulation techniques for next-generation wireless networks," *IEEE Access*, vol. 5, no. 1, pp. 16693–16746, Sep. 2017.

[35] *Study on New Radio (NR) Access Technology*, document 38.912 V14.1.0, 3GPP, Jun. 2017.

[36] Z. E. Ankarali, B. Peköz, and H. Arslan, "Flexible radio access beyond 5G: A future projection on waveform, numerology, and frame design principles," *IEEE Access*, vol. 5, pp. 18295–18309, Mar. 2017.

[37] E. Özturk, E. Basar, and H. A. Çirpan, "Spatial modulation GFDM: A low complexity MIMO-GFDM system for 5G wireless networks," in *Proc. 4th IEEE Int. Black Sea Conf. Commun. Netw.*, Varna, Bulgaria, Jun. 2016, pp. 1–5.

[38] E. Basar, "Index modulation techniques for 5G wireless networks," *IEEE Commun. Mag.*, vol. 54, no. 7, pp. 168–175, Jul. 2016.

[39] E. Ozturk, E. Basar, and H. A. Cirpan, "Generalized frequency division multiplexing with index modulation," in *Proc. IEEE GLOBECOM Workshops*, Washington, DC, USA, Dec. 2016, pp. 1–6.

[40] E. Ozturk, E. Basar, and H. A. Cirpan, "Generalized frequency division multiplexing with space and frequency index modulations," in *Proc. 5th IEEE Int. Black Sea Conf. Commun. Netw.*, Istanbul, Turkey, Jun. 2017, pp. 1–6.

[41] D. Wübben, R. Böhnke, J. Rinas, V. Kühn, and K. D. Kammeyer, "Efficient algorithm for decoding layered space-time codes," *Electron. Lett.*, vol. 37, no. 22, pp. 1348–1350, Oct. 2001.

[42] *Base Station (BS) Radio Transmission and Reception*, document 36.104 V14.4.0, 3GPP, Jun. 2017.

[43] *Multiplexing and Channel Coding*, document 36.212 V14.3.0, Jun. 2017.

ERSİN ÖZTÜRK received the B.S. degree in electronics and communication engineering from Yildiz Technical University, Istanbul, Turkey, in 1995, and the M.S. degree in electronics and communication engineering from Istanbul Technical University, Istanbul, Turkey, in 1998, where he is currently pursuing the Ph.D. degree in telecommunication engineering. His current research areas include waveform design, multicarrier systems, index modulation, and digital signal processing for wireless communications.

ERTUGRUL BASAR (S'09–M'13–SM'16) received the B.S. degree (Hons.) from Istanbul University, Turkey, in 2007, and the M.S. and Ph.D. degrees from Istanbul Technical University in 2009 and 2013, respectively. He was with the Department of Electrical Engineering, Princeton University, NJ, USA, from 2011 to 2012. He was an Assistant Professor with Istanbul Technical University from 2014 to 2017, where he is currently an Associate Professor of electronics and communication engineering. He is an inventor of two pending patents on index modulation schemes. His primary research interests include MIMO systems, index modulation, cooperative communications, OFDM, and visible light communications.

He was a recipient of the Istanbul Technical University Best Ph.D. Thesis Award in 2014. He has received three best paper awards, including one from the IEEE International Conference on Communications 2016. He currently serves as an Associate Editor for the IEEE COMMUNICATIONS LETTERS and the IEEE ACCESS, and an Editor for *Physical Communication* (Elsevier). He is also a regular reviewer for various IEEE journals and has served as a TPC member for several conferences.

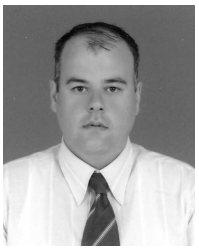

HAKAN ALİ ÇIRPAN (S'95–M'00) received the B.S. degree from Uludag University, Bursa, Turkey, in 1989, the M.S. degree from the Istanbul University, Istanbul, Turkey, in 1992, and the Ph.D. degree from the Stevens Institute of Technology, Hoboken, NJ, USA, in 1997, all in electrical engineering. From 1995 to 1997, he was a Research Assistant with the Stevens Institute of Technology, where he was involved in signal processing algorithms for wireless communication systems. In 1997, he joined the Department of Electrical-Electronics Engineering, Istanbul University, as a Faculty Member. In 2010, he joined the Department of Electronics and Communication Engineering, Istanbul Technical University, as a Faculty Member. His general research interests cover wireless communications, statistical signal and array processing, system identification, and estimation theory. His current research activities are focused on machine learning, signal processing, and communication concepts with specific attention to next generation mobile wireless communication systems. He received the Peskin Award from the Stevens Institute of Technology and the Prof. Nazim Terzioglu Award from the Research Fund of Istanbul University. He is a member of Sigma Xi.